CHEMOTACTIC GRADIENT GENERATOR

A Microfluidic Approach on how
Dictyostelium discoideum Change Direction

Börn Meier

Dissertation
an der Fakultät für Physik
der Ludwig-Maximilians-Universität München

vorgelegt von
Börn Meier
aus Marktredwitz

München, den 9.12.2011

Erstgutachter: Prof. Dr. Joachim O. Rädler
Zweitgutachter: Prof. Dr. Thomas Franosch
Tag der mündlichen Prüfung: 03. Feb 2012

Contents

Kurzzusammenfassung

Die Fähigkeit von Zellen die Quelle eines chemischen Lockstoffs zu erkennen und sich gezielt darauf zu zu bewegen, wird Chemotaxis genannt. Chemotaxis resultiert aus einem hoch entwickelten Zusammenspiel zahlreicher Proteine in einem komplexen Netzwerk. Die experimentelle Identifizierung einzelner biochemischer Signalkaskaden und deren Einfluss auf die chemotaktische Reaktion werden jedoch durch teilweise redundante, parallel verlaufende Reaktionspfade erschwert. Trotzdem versprechen die stetige Weiterentwicklung in der Erzeugung von chemotaktischen Gradienten und deren schnelle Modifikation in mikrofluidischen Flusskammern immer tiefere Erkenntnisse über die Grundlagen der intrazellulären Signaltransduktion.

In dieser Arbeit stelle ich einen chemotaktischen Gradienten Erzeuger (*engl.* Chemotactic Gradient Generator (CGG)) basierend auf einer T-Kreuzungsflusskammer vor. Im CGG werden Zellen mit alternierender Richtung der chemotaktischen Gradienten stimuliert. Eine statistische Auswertung der Zellmigration wird durch eine weite Ausdehnung der chemotaktischen Gradienten ermöglicht. Die Breite des Konzentrationsgradienten von bis zu 300 µm erlaubt es mehrere Dutzend Zellen gleichzeitig anzuregen. Die zur Erzeugung der Konzentrationsgradienten benötigte präzise Kontrolle der Flussgeschwindigkeiten an den einzelnen Zuflüssen der Flusskammer wird durch die Kombination aus Membrandruckpumpen und einer Spritzenpumpe erreicht. Der CGG vereint die Erzeugung homogener Konzentrationsgradienten mit deren effizienter Modifizierung mit einer Schaltfrequenz von bis zu 0.7 Hz.

Das schnelle Umschalten der Gradientenrichtung in unserem Aufbau ermöglicht die Stimulation der Zellen auf der intrinsischen Zeitskala der chemotaktischen Antwort, was durch die schrittweise Erhöhung der Schaltfrequenz gezeigt werden konnte. Bei einer Schaltfrequenz von 0.1 Hz befindet

sich *Dictyostelia discoideum* (*D. discoideum*) in einem Zustand, in dem die Zellen in einer "chemotaktischen Falle" gefangen sind. Dabei ändert sich die Richtung des chemotaktischen Gradienten so schnell, dass die Zellen ihm nicht durch Migration folgen können.

Im Gegensatz dazu reagieren die Zellen mit oszillierenden Bewegungsmustern für Schaltfrequenzen unterhalb von 0.02 Hz. In diesem Fall stehen umpolarisierende Zellen, die nach dem Umschalten der Gradientenrichtung ihren Aktinkortex umbauen, solche Zellen, die ihre Zellfront nur schrittweise neu ausrichten, gegenüber. Um beide Typen experimentell eindeutig unterscheiden zu können, untersuchen wir die Form der Zellen und die intrazelluläre Verteilung der Aktinpolymerisation. Während die Form der Zellen durch ihre Exzentrizität definiert ist, führen wir ein Verteilungsmoment der Fluoreszenz ein um die Aktinpolymerisations-Dynamik zu beschreiben.

Diese quantitative Analyse der chemotaktisch induzierten Migration ermöglicht es, den Einfluss der experimentellen Randbedingungen wie des chemotaktischen Gradienten und der Hungerzeit der Zellen aber im speziellen auch den Einfluss bestimmter Signalproteinen, auf die Zellmigration systematisch zu untersuchen. Dies wird in dieser Arbeit anhand der gezielten Inhibierung von PI3-Kinase mit LY 294002 demonstriert. PI3-Kinase stimuliert die Ausbildung von neuen Pseudopodien und ist somit ein bestimmendes Protein für die chemotaktische Zellantwort.

Sowohl zunehmende Hungerzeit wie auch Gradienten mit reduzierter Steigung induzieren einen geringeren Anteil von umpolarisierenden Zellen, was auf einen verminderten Einfluss von PI3-Kinase auf die chemotaktische Antwort unter diesen Bedingungen schließen lässt. Die Inhibierung von PI3-Kinase mit LY 294002 führt nach 5 h Hungerzeit zu einer abgeschwächten Umpolarisierung der Zellen, während nach 7 h ein positiver Effekt auf das Migrationsverhalten ersichtlich wird. Unsere Ergebnisse deuten auf eine abnehmende Bedeutung von PI3-Kinase mit zunehmender Entwicklung der Zellen während der Hungerphase hin. Es ergibt sich das bemerkenswerte Ergebnis, dass die Inhibierung von PI3-Kinase in Abhängigkeit von den Randbedingungen des Experiments förderlich für effiziente Chemotaxis sein kann. Damit ermöglicht unser chemotaktischer Gradienten Erzeuger erstmals die quantitative Untersuchung des hungerzeitabhängigen Einflusses von PI3-Kinase auf die chemotaktische Antwort von *D. discoideum*.

Abstract

Chemotaxis, the ability of cells to detect and migrate directly towards a source of a chemically active agent, is the result of a sophisticated interplay of proteins within a complex regulatory network. However, partially redundant pathways that simultaneously mediate chemotaxis and dynamic protein distributions complicate the experimental identification of distinct signaling cascades and their influence on chemotactic migration. Yet, increasingly precise generation and rapid modification of chemotactic stimuli in microfluidic devices promise further insight into the basic principles of cellular feedback signaling.

I developed a Chemotactic Gradient Generator (CGG) for the exposure of living cells to chemotactic gradient fields with alternating gradient direction based on a double T-junction microfluidic chamber. A large extension of the concentration gradients enables the parallel exposure of several dozens of cells to identical chemotactic stimuli, allowing for a reliable quantitative analysis of the chemotactic migration behavior. Two pressure pumps and a syringe pump facilitate accurate control of the inflow velocities at the individual flow chamber inlets, pivotal for precise manipulation of the chemotactic stimuli. The CGG combines homogeneous gradients over a width of up to 300 µm and rapid alterations of gradient direction with switching frequencies up to 0.7 Hz.

Fast gradient switching in our experimental design facilitates cell stimulation at the intrinsic time scales of their chemotactic response as demonstrated by a gradual increase in the switching frequency of the gradient direction. We eventually observe a "chemotactically trapped" state of *Dictyostelium discoideum* (*D. discoideum*) cells at a switching rate of 0.01 Hz. Here, gradient switching proves too fast for the cells to respond to the altered gradient direction by migration.

In contrast, we observe oscillatory runs at switching frequencies of less than 0.02 Hz. We distinguish between re-polymerizing cells that exhibit an internal re-organization of the actin cortex in response to chemotactic stimulation and stably polarized cells that gradually adjust their leading edge when the gradient is switched. To experimentally characterize both response types, we record cell shape and the intracellular distribution of actin polymerization activity. Cell shape is readily described by the eccentricity of the cell and to record F-actin polymerization dynamics we introduce a fluorescence distribution moment (FDM).

Accurate description of the migratory response behavior facilitates a quantitative analysis of the influence of both the experimental boundary conditions such as gradient shape, ongoing starvation of the cells, and in particular the influence of distinct signaling cascades on chemotactic migration. Here, we demonstrate this ability of the GCC by inhibition of PI3-Kinase with LY 294002. PI3-Kinase initiates the formation of fresh pseudopods in the direction of the chemotactic gradient and therefore is one of the key signaling pathways mediating the chemotactic response.

In shallow gradients and with ongoing starvation of the cells, we find a decreased ratio of re-polymerizing cells, pointing towards a diminished influence of PI3-Kinase. After inhibition of PI3-Kinase, cell re-polymerization in response to a switch in gradient direction is hindered at 5h of starvation, whereas at 7h of starvation evidence is found that chemotactic migration is more efficient. We observe the astonishing result that in dependency of the boundary conditions of the experiment inhibition of PI3-Kinase promotes an effective chemotactic response.

Thus, the CGG for the first time facilitates a quantitative analysis of the starvation time dependent effect of PI3-Kinase inhibition on *D. discoideum* chemotaxis.

Chapter 1

Introduction: Exploring Regulatory Networks of Cells

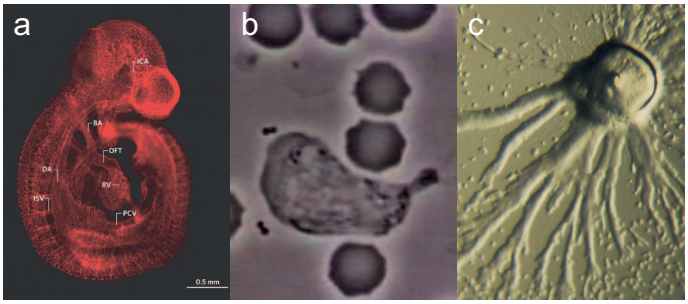

Figure 1.1: Chemotactic gradients in embryogenesis, angiogenesis, immune response and aggregation of *D. discoideum*: (a) The organization of a developing organisms such as an embryo depends on complex interaction of gradients determining cell differentiation (Fig. 1 in [1]) . (b) A leukocyte is chasing a bacterium, tracking down its chemical footprint (David E. Rogers, Vanderbilt University). (c) The social amoebae *D. discoideum* aggregates by releasing the chemoattractant cAMP (by Bruno in Columbus, via Wikimedia Commons).

Cells are sophisticated assembly lines for proteins [2], molecular force generators [3] and highly sensitive chemical sensors [4]. Understanding the basic feedback principles underlying the intracellular regulatory network remains one of the big challenges of life science.

Inspired by the demanding goal to identify key signaling cascades in cells' complex and partially redundant molecular pathways [5], steady improvements in the experimental and theoretical description of cell responses have been achieved. The introduction of the green fluorescent protein (GFP) in

1994 for example, revolutionized quantitative analysis of protein distributions in living cells [6]. Fluorescence microscopy with genetically encoded proteins facilitated the description of dynamic cell response, as fluorescence markers can be tracked over time on a molecular level. As a result, rapid imaging of the dynamic intracellular protein distribution has become possible. Still, stochastic gene expression [7] and the resulting wide statistical spread in individual cell responses [8] impede easy access to the input-output functions of the regulatory network of living cells. Precisely tuned perturbations that excite the intracellular feedback are pivotal for further investigation of cell response. Improving the visualization of intracellular signaling events is only meaningful if the temporal resolution of the experimentally applied cell stimuli is also advanced.

Generating chemotactic gradients

Diverse external stimulation can possibly be used to experimentally probe cell response during electrotaxis, mechanotaxis and chemotaxis. Electric stimulation is, for example, easily tuned at very fast time scales, however application to cells in the ubiquitous moist environment remains difficult [9, 10]. Mechanical stimulation such as gradually increasing stiffness or adhesion area at the cell substrate [11] can be presented to the cells without great difficulty, but temporal manipulation is constricted to a few specialized experiments [12].

In contrast, chemotaxis, the ability of cells to migrate towards or away from a source of a chemical analytic, appears to be ideally suited to explore intracellular feedback. Pioneering assays generated chemical gradients utilizing micropipettes [13] or diffusion chambers [14, 15]. Microfluidic mixing in labyrinth-like structures [16, 17] and optically manipulated nanocapsules [18] improved the definition and manipulation of chemical gradients, while microfluidic T-junctions [19] or photo-induced release of a chemotactic stimulant [20] have been used to expose cells to a rapid, global rise in chemoattractant. Chemical stimulations are readily tuned with sub-cellular precision [21] and on time scales from fractions of a second to several hours [22].

Still, not only the straightforward experimental handling of chemotactic stimuli but also its importance in life science brought eukaryotic chemo-

taxis into the focus of scientific investigation. Chemotaxis is, among other factors, pivotal for the development of entire complex organism during embryogenesis [1], the tracking down of invading bacteria by leukocytes [23] or the aggregation process of the social amoebae *Dictyostelium discoideum* [24] (Fig. 1.1).

Chemotaxis in *Dictyostelium discoideum*

D. discoideum is a particular ideal model system due to its relative ease in handling and its genetic congruence to mammalian cells [25]. It provides not only an interesting system of study in regards to vital cellular functions such as migration [26], food gathering [27] or cell differentiation [28], but also elucidates the general principles of intracellular signaling [29]. Consequentially, the genome of *D. discoideum* has been among the first to be analyzed and many of its key players in chemotactic feedback can be genetically manipulated by now [30, 31]. As an exceptional sensor working at the lower limit of detectable signal-to-noise ratio [32] and over several orders of magnitude of background concentration [33], *D. discoideum* demonstrates an amazing robustness of the chemotactic regulatory system.

Easy handling of chemotactic gradients and the great general interest in eukaryotic chemotaxis led to a vast knowledge about the proteins involved in its regulatory network [34]. Yet, a detailed understanding on how distinct signaling pathways interact with each other to enable the sophisticated feedback control of the chemotactic response is still missing. To research the basic principles of intracellular feedback, mathematical modeling based on the experimental observation of the chemotactic response of *D. discoideum* has been established [35, 36, 37]. Recent models address time-dependent chemotactic stimuli and migratory cell response to a change in gradient direction. The obtained, increasingly complex input-output relations result in new challenges for the experimental description of chemotactic migration [38, 39].

The Chemotactic Gradient Generator

In this thesis, I have developed a Chemotactic Gradient Generator (CGG) for the stimulation of living cells with alternating sequences of chemotactic gradient fields of opposing direction. Experiments are conducted at low

flow velocities of $1\,^{mm}/_{s}$, which facilitates the generation of homogeneous concentration gradients that extend over several hundred microns, but still permit rapid modification of the gradient direction. Accurate control of the inflow velocities enables an increase of the switching frequency between two chemotactic gradient fields up to the point where cell migration is inhibited and 90% of the cells remain in a "chemotactically trapped" cell state. Chemotactic cell trapping establishes the capability of the CGG to excite the cells on the intrinsic time scales of directional sensing.

Previous reports describe two types of migration behavior in response to changes in the direction of the chemotactic gradient. The first type is determined by re-polymerizing cells that re-organize their actin cortex, forming a new leading edge by PI3-Kinase based formation of a fresh pseudopod, whereas the second migration type keeps a stable polarization and gradually adjusts its migration direction by Phospholipase A2 (PlA2) based splitting of the leading edge. It is known that both pathways simultaneously mediate the chemotactic response [40], but how the initial conditions of the chemotactic stimulus, such as gradient steepness or starvation time, influence chemotactic migration is still under investigation [41]. The large extension of the chemotactic gradients in the CGG, allows for simultaneous excitation of dozens of cells with identical chemotactic stimuli, facilitating the necessary sample numbers for a reliable analysis of the migratory response behavior dependent on theses parameters.

To access the influence of cell starvation and gradient steepness on chemotactic migration, we introduce a fluorescence distribution moment (FDM) for the Gfp fusion protein of the actin polymerization promoter LimEΔcc and determine the cell orientation with respect to the chemotactic gradient. FDM analysis is ideally suited to quantify the chemotactic response of the first migration type involving re-polymerizing cells, whereas cell orientation with respect to the chemotactic gradient is used to investigate the migration of the second type.

We find oscillatory runs at lower switching frequencies, allowing for a quantitative analysis of the migratory behavior in response to a change in the direction of the chemotactic gradient. In shallow gradients and with ongoing starvation of the cells we observe an increased number of cells of the second migration type . Our results suggest that with ongoing starvation,

the first migration type, which is primarily based on the PI3-Kinase mediate formation of fresh pseudopodia, becomes less significant for chemotactic migration. Experiments that introduce a pharmacological perturbation of PI3-Kinase to the cells underline this assumption. We, for the first time, determine the influence of PI3-Kinase on the chemotactic migration of *D. discoideum* as it depends on the starvation of the cells. For $5-6\,\mathrm{h}$ of starvation, cells perturbed in PI3-Kinase are found to be less efficient in rearranging their actin polymerization activity after a switch in the direction of the chemotactic gradient, whereas for $6-7\,\mathrm{h}$ of starvation, PI3-Kinase perturbation even promotes effective response to alternating chemotactic gradients.

Chapter 2

Model System for Eukaryotic Chemotaxis: *Dictyostelium discoideum*

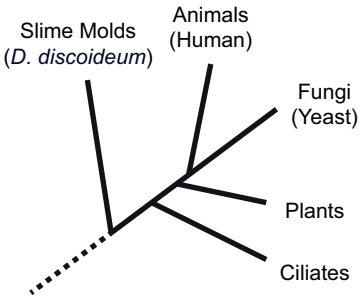

Figure 2.1: Its genetic diversity makes *D. discoideum* a widely accepted model for eukaryotic chemotaxis. *D. discoideum* split of from early in their evolutionary history but kept much of their genomic diversity [30, adapted from Fig. 5], resulting in a closer genetic relationship to mammalian cells than is observed, for example, in yeast cells.

Dictyostelium discoideum is a soil-living social amoeba, often referred to as slime mold, which belongs to the phylum *Mycetozoa*. *D. discoideum* split off early in its evolutionary process but much of its genetic diversity has been conserved and it has been found to contain more mammalian gene homologs than yeast, which is widely accepted as a model system for eukaryotic cells (Fig. 2.1) [42, 43]. Furthermore, many of the chemotactic signaling pathways that are later found in leukocytes have been elucidated in *D. discoideum* [25]. *D. discoideum* exhibits notable advantages over mammalian

cells in live cell experiments:

- *D. discoideum* is a haploid organism and its genome has been decoded [30], giving access to many genetically manipulated variations with genes knocked out, over-expressed or fluorescently tagged, which are freely available at the Dicty Stock Center [31].
- *D. discoideum* are simple to harvest in relatively cheap medium and rapidly grown to large densities yielding easy access to live cell experiments at room temperature.
- Its unique life cycle with a known onset of starvation allows for the definition of precise initial conditions in chemotactic experiments.

2.1 Life cycle of *Dictyostelium discoideum*

The *D. discoideum* life cycle starts with the free living amoebae, referred to as vegetative cells, gathering food by chasing bacteria. When confronted with starvation, the single amoebae undergo a series of morphological changes eventually assembling in complex multi-cellular organisms to form spores (Fig. 2.2) [24].

In more detail, the unicellular living amoebae feed on bacteria and proliferate by mitosis until the depletion of food sources initiates cell development that sensitizes the cells to stimulation with the chemoattractant cyclic Adenosin-3´,5´-monophosphat (cAMP). After $4-5$ h of starvation the single amoebae start to release cAMP on their own [44]. At $5-7$ h of starvation the cells pass into the aggregation mode. The still unicellular migrating cells polarize by the formation of a leading edge and an uropod. During this phase, the amoebae change from an unbiased amoebic migration to a biased migration that is directed by external cAMP concentration gradients. After8 h of starvation the multicellular developmental phase initiates with the formation of aggregation centers containing several hundreds of thousands of cells [45]. After approximately 16 h, multicellular slugs, capable of coordinated migration, emerge. Within these slugs, cells differentiate. Some of the cells emerge to form the stalk of a fruiting body, at the head of which others form spores. The fruiting body is completed approximately 24 h after starvation is initiated. When new food sources emerge the spores sprout

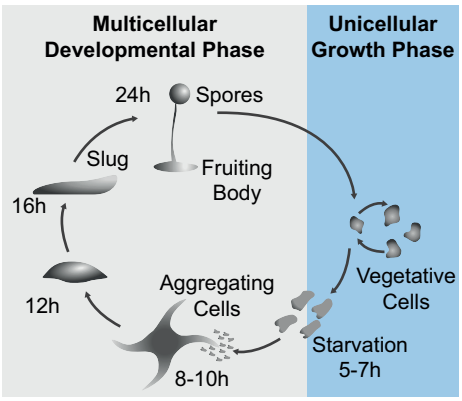

Figure 2.2: Life cycle of *D. discoideum*. When the free living single amoebae (unicellular growth phase in blue) faces starvation it starts to aggregate after $5-7\,\mathrm{h}$. The single cell undergoes a series of morphological changes, eventually forming a multicellular organism to produce spores, thus ensuring survival of a new generation of slime mold (multicellular developmental phase in gray) [24, adapted from Fig. 1].

and the *D. discoideum* life cycle starts over, ensuring a new generation of slime mold.

In this thesis, I use cells at the onset of chemotactic migration that have been starved for $5-7\,\mathrm{h}$. During the transition from vegetative cells ($< 6\,\mathrm{h}$) to aggregating cells ($< 6\,\mathrm{h}$), the single amoebae exhibit a chemotactic behavior that is typical for unicellular living eukaryotic cells. The unique life cycle of *D. discoideum* allows for a precise timing of the starvation phase of the cells by depletion of the food source, and therefore the initial condition of the experiment.

2.2 The Three Steps of Eukaryotic Chemotaxis

Chemotactic migration arises from a bias in regular "random" migration towards the direction of the chemotactic gradient. A chemotactic cell has to identify the direction of the external concentration gradient, couple this information to its migratory apparatus and form protrusions in the desired direction.

On a molecular scale, cAMP binds to the membrane bound cAR receptor that is itself coupled to heteromeric G-proteins. The cyclic AMP receptor

Intracellular Signaling at the leading edge	
PI3-Kinase	PI3-Kinase phosphorelates PIP2. The phosphorylation of PIP3 in the direction of the gradient is the main pathway described to act as a chemotactic compass.
PIP3	Membrane bound phospholipid that promotes actin polymerization. If PIP3 is present at the membrane, actin polymerization is enhanced.
Cell migration	
F-actin	Globular actin (G-actin) is the building block of filamentous actin (F-actin) that emerges by polymerization of G-actin monomers. The actin filaments are cross-linked to form actin networks that, for example, protrude pseudopods in cell migration.
Suppression of lateral pseudopods	
cGMP	Small messenger protein with a high diffusion coefficient that is proposed to induce a global inhibition of pseudopod extension.
PTEN	Degenerates PIP3 to PIP2. Accumulates at the cell's rear, hindering accumulation of PIP3 and therefore the extension of lateral pseudopodia.
Myosin II	Molecular motor, involved in the contraction of the actin cortex allowing for efficient retraction of the rear.

Table 2.1: Proteins and signaling molecules and their importance for the single steps in the chemotactic response of *D. discoideum*

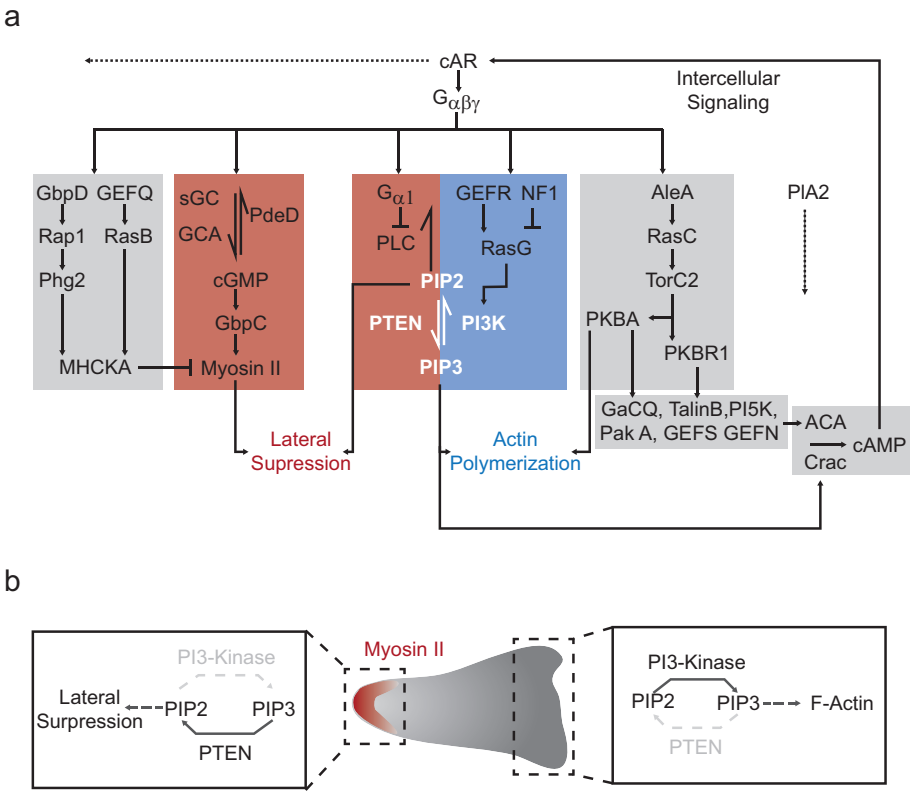

Figure 2.3: Regulatory network of the chemotactic response in *D. discoideum*. (a) G proteins connected to the cAMP receptor cAR simultaneously activate multiple signaling cascades that are involved in the chemotactic response. In this theses I concentrate on the influence of the PIP2/PIP3 gradient on the actin polymerization dynamics in response to altered chemotactic stimulation. PIP3 is generated by PI3-Kinase, whereas PTEN degenerates PIP3 to produce PIP2 (highlighted in white). Signaling cascades that are directly involved in the polymerization of filamentous actin are mostly well described, whereas feedback schemes based on phospholipid signaling, for example PlA2, are not yet connected to the residual response (adapted from Fig. 4 in [46]). (b) A concentration gradient of PIP3 and PIP2 is likely to mediate cell polarization. At the leading edge of the cell, PI3-Kinase produces PIP3, which enhances the polymerization of F-actin. At the rear of the cell PIP3 is degenerated by PTEN to PIP2, hindering the formation of pseudopods. The accumulation of Myosin II (red) at the uropod, further retracts the cell's rear, thereby impeding lateral pseudopodia.

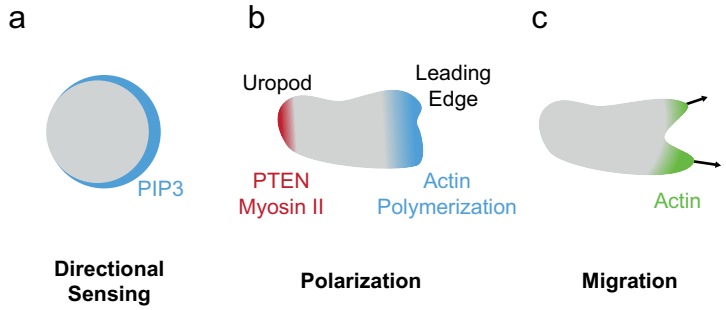

Figure 2.4: The three separate steps of (a) directional sensing, (b) polarization and (c) migration are distinguished in *D. discoideum* to facilitate qualitative description of the chemotactic response. (a) The process of directional sensing describes the intracellular reproduction of the chemotactic gradient by the membrane bound phospholipid PIP3 (blue). (b) During the polarization process, actin polymerization enhancing proteins accumulate at the leading edge (blue), whereas lateral pseudopod extension is hindered by the accumulation of PTEN and Myosin II at the uropod (red). (c) The spatial information of the chemotactic gradient is connected to the migratory apparatus of the cell by the polymerization of F-actin. The cell forms pseudopods in the direction of the chemotactic gradient (green).

(cAR) as well as diverse G-protein sub-domains initiate multiple parallel signaling cascades that determine the response of the cell's front and rear. The cell perimeter pointing towards the chemotactic stimulus is defined by the polymerization of filamentous actin (F-actin) that leads to the extension of cell protrusions. At the uropod of the cell Myosin II accumulates, contracting the cell's rear and thereby preventing the formation of lateral pseudopodia [47] (see Fig. 2.3).

In my thesis, I concentrate on the generation of a concentration gradient of the membrane bound phospholipid phosphatidylinositol (3,4,5)-trisphosphate (PIP3) through the phosphorylation of phosphatidylinositol (4,5)-bisphosphate (PIP2) by phosphoinositide 3-kinases (PI3-Kinase) at the cell front and the degeneration of PIP3 at the uropod by the phosphatase and Tensin homolog PTEN [48]. PI3-Kinase accumulates at the side of chemotactic stimulation, which is essential for the formation of new pseudopods [49], whereas PTEN is mainly observed at the rear of the cell, adding to the suppression of lateral pseudopodia [50].

Overall, most signaling cascades known to participate in chemotactic migration are based at Ras signaling molecules, however the already complex picture of regulatory networks has recently been supplemented by phospho-

lipid signaling. Particularly, Phospholipase A2 (PlA2) based splitting of the leading edge is shown to significantly influence chemotactic response, although the mechanism for pseudopod splitting remains unknown.

In summary, we find an elaborate, partially unresolved, biochemical network to control the chemotactic response of *D. discoideum*. It has, however, remained impossible to experimentally or theoretically address the chemotactic regulatory network in its full complexity. Consequently, chemotactic response is often divided into the three separate processes of **directional sensing**, **polarization** and **migration**, to enable a quantitative description (Fig. 2.4) [51].

The extension of cell protrusion depends on the polymerization of filamentous actin (F-actin) [52, 53]. Therefore, the amount of F-actin can be used as a measure for the chemotactic activity of the cell [54]. Chen at al. find a characteristic F-actin polymerization behavior in response to a uniform increase in cAMP concentration. A pronounced but narrow increase in the amount of F-actin in the cell, 10 s after chemotactic stimulation, is followed by a less pronounced but much broader peak of F-actin polymerization at approximately 120 s. Both F-actin peaks can be experimentally related to **directional sensing**, and **migration**.

Directional sensing describes the ability of eukaryotic cells to establish an intracellular replication of an external concentration gradient. Experiments that expose the cells to uniform pulses of the chemoattractant measure a rise in the concentration of PIP3, which is followed by the polymerization of actin at the cell cortex within 10 s [55]. The PIP3 gradient is called the chemotactic compass of the cell, as it is the first intracellular marker for the direction of the chemotactic gradient [56]. In contrast to bacteria that depend on motion to identify a rise in chemoattractant concentration over time [57], eukaryotic cells recognize the concentration drop between leading edge and rear of the cell [4]. Cells that are deficient in the formation of F-actin due to treatment with Latrunculin still built up an accumulation of PIP3 in the direction of the chemotactic gradient. The formation of a concentration gradient in PIP3 in cells that are unable to migrate, proves the ability of *D. discoideum* to spatially resolve the chemotactic gradient independently of cell migration [58].

Polarization of the cell describes the accumulation of actin polymer-

ization enhancing proteins to the side of chemotactic stimulation, and the recruitment of proteins that are necessary for the retraction of the cells rear to the so called uropod [59]. During this process, the external chemotactic gradient is amplified within the cell resulting in a steeper intracellular concentration gradient than is provided by the external chemotactic gradient [60]. The accumulation of PIP3 at the membrane recruits actin polymerization enhancing proteins [61] such as the actin crosslinker Arp2/3 [62] or the actin capping protein Coronin [52] to the site of stimulation, thus initiating the formation of a new pseudopod. At the rear of the cell, PTEN perturbs PIP3 accumulation, preventing lateral pseudopods [63]. Additionally, the recruitment of the motor protein Myosin II to the cell's rear is observed which is responsible for the retraction of uropod [64].

The molecular pathways and intracellular distribution of *D. discoideum* are already well established for a large fraction of the proteins known to be involved in the chemotactic response. Yet, it is still under investigation how *D. discoideum* manages to establish and maintain an internal polarization in response to a chemotactic gradient. While directional sensing of the chemotactic gradient is apparently linked to the intracellular distribution of PIP3, the signal propagation to the uropod is not as clear-cut. To maintain a concentration gradient of a distinct molecule within a single cell, the protein must have both, a small diffusion coefficient and a short lifetime. Exemplary, this is the case for the membrane bound PIP3, which is therefore ideally suited to conserve the spatial information of the chemotactic gradient. In contrast, a messenger molecule that has to carry the chemotactic stimulation to the cell's rear must to have a large diffusion coefficient since a large distance needs to be bypassed. One protein possibly mediating the inhibitory feedback is Cyclic guanosine monophosphate (cGMP) [65, 66, 67]. Still, it should be noted that a negative feedback mechanism, based on a small quickly-diffusing molecule, cannot be confined to the cell's rear and would therefore also inhibit the formation of cell protrusions at the cell front [68]. Consequentially, the mechanism of pseudopod suppression at the rear of the cell is under debate and alternative schemes such as membrane tension exerted by an emerging pseudopod at the cell front carrying the information to the uropod, have also been considered (plenary talk of O. Weiner at *Dictyostelium discoideum* 2010, Cardiff).

Migration denotes a cell's ability to actively and directly propel itself in the direction of a chemotactic stimulus. The second much broader but less intense peak in F-actin polymerization is connected to the actual formation of pseudopods [54]. During the 120 s before the first pseudopods are extended in the direction of the chemotactic gradient, the cell establishes a local polarization in chemotaxis related proteins. At the cell front, actin polymerization is enhanced whereas the rear of the cell, the uropod, is contracted, eventually resulting in a bias of the migration direction [47]. Through theses mechanisms, the cell translates the information gained by both sensing and amplification of the chemotactic gradient into actual locomotion.

To conclude, most of the proteins involved in directional sensing, polarization and migration are biochemically identified and well described [34, 69, 70]. Furthermore, the intrinsic time scales for the feedback motifs of directional sensing and polarization are found to be 10 s and 120 s, respectively [54].

2.3 Modeling Eukaryotic Chemotaxis

In the previous section, I used the signaling-centered view to describe the basic principles of chemotactic migration. However, besides the already mentioned uncertainties on how a particular chemotactic stimulation is communicated between the front and the rear of the cell, the main pathway representing the intracellular chemotactic compass, PI3-Kinase based accumulation of PIP3 at the cell membrane, has recently been challenged [71, 72, 73]. Only the knockout of multiple proteins, including PI3-Kinase and PlA2 among several others, results in severe chemotactic defects, pointing towards multiple parallel pathways that mediate the chemotactic response [74, 75].

Furthermore, previous experiments exposing the cells to changes in the direction of the chemotactic gradient reveal two fundamentally different migratory behavior [41, 40]. Cells tend to form a new pseudopod if the altered gradient is steep (Fig. 2.5, left), whereas if a weaker gradient is applied, the cells keep their prior pseudopods and perform a "U-turn" to follow the chemotactic stimulation (Fig. 2.5, right). The signaling-centered

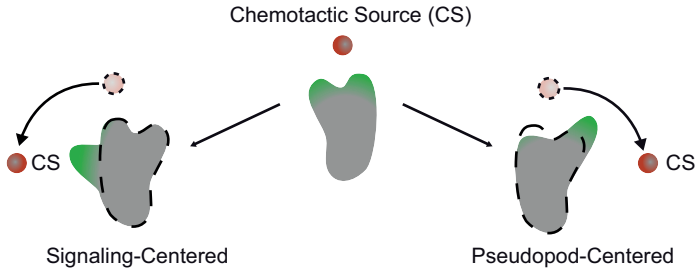

Figure 2.5: Migratory response of *D. discoideum* as described by the signaling and the pseudopod-centered view. Two fundamentally different cell responses are observed as a result of changing the position of the chemotactic source. The first migration type that is mathematically described by signaling-centered description results in the formation of a fresh pseudopod at the cell side facing the new position of the chemotactic source (left). The pseudopod-centered view describes the second migratory type, where the cell does not form a fresh pseudopod but rather the growth rates of the existing pseudopods is biased (right). Pseudopods that are closer to the chemotactic source are extended, whereas pseudopods that are further away are retracted more quickly.

view, as outlined in the previous section, is the most prominent description of eukaryotic chemotaxis but alternative explanation of chemotaxis, such as the pseudopod-centered view [38], have evolved to describe migratory behavior that differs from the signaling-centered description.

The signaling-centered view

The LEGI (Local Excitation, Global Inhibition) model uses the combination of both a positive and negative feedback loop to describe directional sensing that eventually leads to the formation of a new pseudopod. A rapid, local positive feedback at the side of stimulation results in a fast and pronounced response peak at the leading edge, whereas a more slowly reacting but global inhibition perturbs extension of lateral pseudopods and restricts the positive feedback to the cell front. However, the slower but global rise of the inhibition process also stops the excitation at the cell front, preventing a stable polarization of the cell.

Cell polarization is only obtained when the strength of the positive feedback at the cell front is increased. However, a strong positive feedback loop is self-preserving, depleting the ability of the cell to adapt to alterations of the chemotactic excitation [51].

Overall, the LEGI model predicts the formation of a new pseudopod

in the direction of the chemotactic stimulus. A hypothetical cell acting in agreement with the LEGI model would form a fresh pseudopod if the direction of the chemotactic gradient is changed (Fig. 2.5, left). Furthermore, recent expansion of the LEGI model which adds intrinsic noise to the feedback [39], reproduces the migratory behavior of cell deficient in distinct signaling proteins. However, descriptions based on the signaling-centered view result in cells that are not capable of maintaining a cell polarization or adapting to a change in the direction of the chemotactic stimulation.

The pseudopod-centered view

In the second proposed migration type, cells keep their previous leading edge in response to a change in the direction of the chemotactic gradient. This pseudopod-centered view explains this migratory behavior by self-induced pseudopodia [38, 76, 77]. Here, the chemotactic stimulus does not result in the formation of new pseudopods, rather the pseudopod growth phase itself is biased.

The pseudopod-centered view is supported by the experimental observation that the amount of pseudopods formed over time does not depend on chemotactic stimulation [40, 78]. However in the pseudopod-centered view, the growth phase of the pseudopods is biased in a way that pseudopods pointing in the direction of the chemotactic gradient are extended, whereas misleading pseudopods are rapidly retracted. As a result, the cell will gradually turn into the direction of the chemotactic gradient.

The pseudopod-centered view is comparable to the run and tumble motion of bacteria. in which they use a biased random walk to follow an external concentration gradient. The bacteria tumble and afterward swim in randomly distributed directions, however the average run length between two tumble phases is prolonged if the cells approach the chemotactic source and shortened if the cell loses its track. This leads to an overall approach of the bacteria to the chemotactic source.

To conclude, the pseudopod-centered view readily describes the migratory behavior of stably polarized cells, but it cannot explain the formation of fresh pseudopods and the accumulation of PIP3 at the side of chemotactic stimulation.

Experimental validation of mathematical predictions

Both migratory behaviors are readily explained by one of the two mathematical descriptions, but a deeper insight on the mechanism of which migratory response is favored dependent on the chemotactic gradient is still missing. It should also be noted that for both theoretical views on eukaryotic chemotaxis, experimental observations can be brought into agreement with the mathematical descriptions dependent on the initial conditions of the experimental setup. However, a broader statistical analysis and more complex experimental stimulation of the cells is needed to gain further insight into the underlying chemotactic feedback motifs and to validate theoretical predictions.

Chapter 3

Experimental Investigation of Chemotactic Response

Development of sophisticated mathematical models and the increased complexity of the biochemical network known to control chemotactic migration in eukaryotic cells have motivated improvements of experimental assays for the generation of chemotactic stimulation. Diffusion chambers [14, 15], microspheres [18] and gradient mixing in PDMS-based flow chambers [16, 22, 17] improved the shape of the concentration gradients, whereas flow photolysis [20] and microfluidic T-junctions [19] allow for rapid stimulation of the cells. As a next step, the generation of homogeneous concentration gradients needs to be combined with their rapid manipulation.

3.1 Generating Chemotactic Gradients

Pioneering micropipette assays [13]

The most prominent tool to chemotactically stimulate starved cells is the micropipette (Fig. 3.1a). The micropipette is brought close to the cell ensemble, acting as a point source of a particular chemoattractant. Based on diffusion, a spherical but nonlinear gradient evolves within a few seconds. The micropipette features very steep gradients adjacent to the tip and rather shallow gradients at the edge of the observation area. Manipulation of the emerging gradients is restricted to the chemoattractant concentration within the micropipette and its distance to the investigated cells. The micropipette

yields quick access to a large number of cells, but the cells are exposed to gradients with varying steepness and a rising background concentration.

Microspheres [18]

Optical trapping of microspheres loaded with chemoattractant allow for precise shaping of complex concentration landscapes for single cells. Krees et al. were able to manipulate several microspheres at once and dynamically move them within the observation area. The nanoporous beads emit chemoattractant much like a micropipette, generating a gradient field by diffusion (Fig. 3.1b). Multiple microspheres in the vicinity of a single cell, produce complex gradient landscapes that can dynamically be manipulated by rapid repositioning of single spheres.

Diffusion chambers [14, 15]

The generation of stationary, linear concentration gradients became possible with the development of diffusion chambers, such as the Boyden or the Dunn chamber (Fig. 3.1c). In principle, two reservoirs each containing a different concentration of chemoattractant are connected through a small bridge to prevent mixing despite diffusion. Over the course of a few minutes a linear gradient evolves and the cells that are placed at the bridge are exposed to a stable linear gradient that, in contrast to micropipette assays, exposes all cells to chemotactic gradients of identical gradient steepness.

3.2 Shaping Chemotactic Stimuli in Microfluidic Flow Chambers

Stationary gradient generators like micropipettes and diffusion chambers are popular as experiments are readily performed and qualitative descriptions of chemotactic phenotypes are easily obtained. However, precise manipulation of the chemotactic gradient is limited as micropipettes generate an inhomogeneous gradient profile and the long equilibration time of diffusion chambers prevent rapid alterations of the gradient.

In contrast, the steady flow in microfluidic flow chambers facilitates rapid manipulation of the concentration gradients in the cell's vicinity and allows

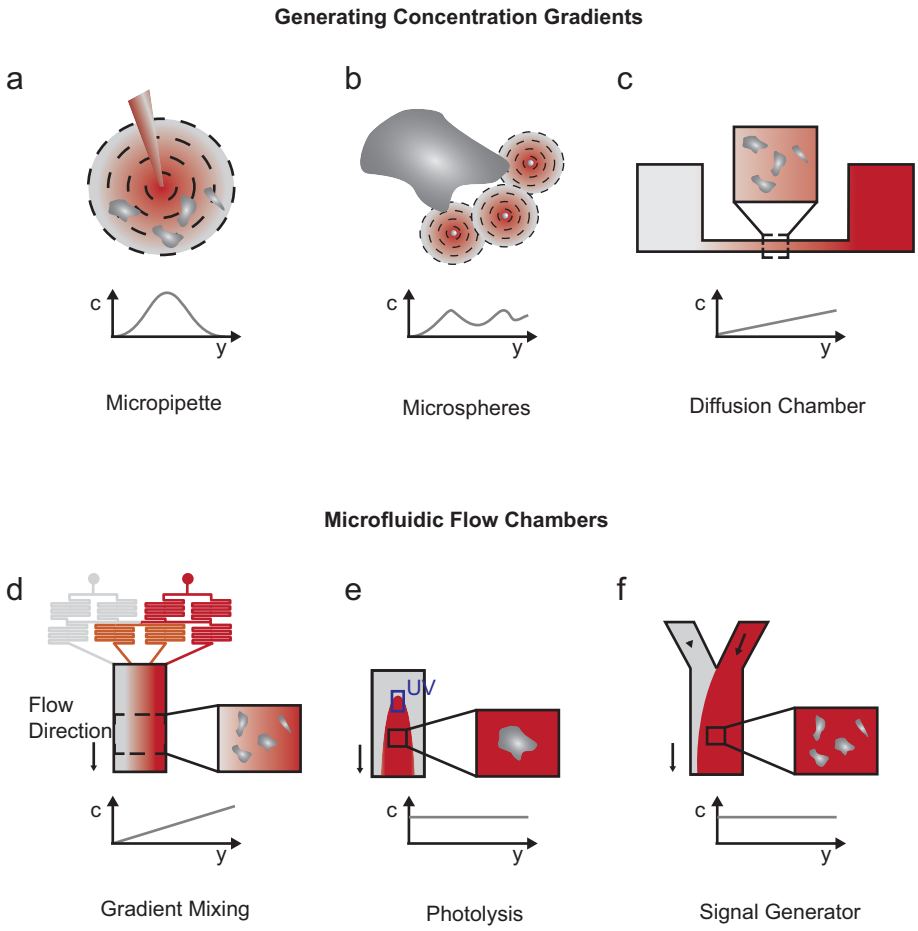

Figure 3.1: A large variety of different experimental assays has been designed to produce chemotactic stimulation (red): (a) Micropipette assays generate non-linear, spherical gradients by diffusion. The concentration profile is defined by a steep gradient at the tip of the cell and more shallow gradients with increasing distance to the tip [13]. (b) Gradient generation with multiple microspheres allows for the precise shaping of the concentration landscape in the vicinity of an individual cell. The microspheres are optically trapped and several beads can rapidly be moved to dynamically excite the cells [18]. (c) The principle of diffusion chambers like the Boyden or Dunn chamber [14, 15], based on a narrow bridge, connecting two reservoirs each containing chemoattractant at different concentration. A linear gradient evolves over the course of a few minutes . (d) Gradient mixing in labyrinth-like structures allow for the generation of linear gradients upstream the flow chamber. The addition of supplemental labyrinth branches facilitates more complex-shaped concentration distributions, such as ramped gradients [16, 22, 17]. (e) Releasing a caged chemoattractant by UV laser light upstream from an individual cell allows for stimulation with rapid pulses of chemoattractant over durations of less than $1s$. Asymmetric UV light patterns also facilitate concentration gradients [20]. (f) Fast switching between two streams becomes possible at high flow velocities with the chemical signal generator [19].

for the generation of identical stimuli over a long time span as remnants off previous stimuli are constantly removed. The inherent laminar flow further promotes precisely controlled gradient mixing at the stream interfaces. The introduction of poly-dimethylsiloxane (PDMS), a polymer that allows for accurate construction of microfluidic flow chambers by soft lithography, greatly advanced the development microfluidic systems, allowing for a huge variety of experimental designs [22]. Microfluidic systems combine many advantages of great importance in the investigation of eukaryotic chemotaxis:

- steady addition of nutrients by a constant flow ensuring a comfortable cell environment for the entire experiment up to several days,
- reproducible chemotactic stimulation as remnants of previous stimulation are removed,
- precise positioning of soluble analytics with sub-cellular resolution [21],
- controlled generation of concentration gradients at the stream interfaces via diffusion.

The flexibility of PDMS flow chambers has resulted in the evolution of a variety of different experimental designs within the last decade.

Gradient mixing in labyrinth-like microfluidic systems [16, 17, 22]

Due to the laminar flow in microfluidic devices, strategies need to be evolved to control the shape of the concentration gradient. A very elegant way is the use of labyrinth-like structures that take advantage of the diffusion between two neighboring streams containing different concentrations of a chemoattractant (Fig. 3.1d). The streams are merged and split repeatedly to generate homogeneous gradients before the observation region is reached. Adding additional branches to the mixing labyrinth not only allows the shaping of linear gradients but also the ability to form steps in the concentration profile [16]. The usage of two different labyrinth systems which are alternatingly connected to the observation area further allow for switching of the gradient direction [17].

Flow photolysis [20]

Activating a caged chemoattractant with laser light, facilitates highly dynamic excitation of individual cells (Fig. 3.1e). Beta et al. have shown that repeated uniform pulses of a caged chemoattractant with duration of less than 1 second can be generated. The chemoattractant is uncaged by a pulse of a UV laser directly upstream from the targeted cell within a microfluidic chamber. By using alternative shapes of laser excitation, Beta et al. have also generated gradients of chemoattractant.

Chemical signal generator [19]

The chemical signal generator exposes entire cell ensembles to a rapidly changing concentration of a chemically active agent. Cells are subjected to fast on-off concentration switches by the alternation between two streams of a T-junction microfluidic chamber (Fig. 3.1f). Here, entire cell ensembles are exposed to the same stimulus. However, fast alternation of the streams requires high flow velocities that can also prevent stimulation of the cell with concentration gradients ([79], also see section 5.5).

Chapter 4

Quantifying the Chemotactic Input-Output Relation

Progress in the experimental stimulation of chemotactic cells facilitates a more quantitative analysis of the chemotactic response. Yet, a precise investigation of the chemotactic input-output behavior as is necessitated by recent theoretical descriptions, requires further improvements of available experimental designs. In the following chapter, I will point out the requirements for an accurate experimental description of the chemotactic response behavior and define the resulting demands for newly developed experiments.

4.1 Identifying Feedback Motifs in the Stochastic Cell Response

The mathematical description of eukaryotic chemotaxis is mainly based on intracellular signaling cascades. Yet, the identification of position and importance of a distinct signaling molecule within the regulatory network is complicated by the variability of response behaviors, possibly generated by only one single feedback loop [81]. A negative feedback might result in an adaption process or convert a constant input into a transient pulse, whereas a simple positive feedback loop can lead to an acceleration of the external signal or even a bistable response depending on the initial condition of the stimulation. More complex experimentally observed feedback dynamics such as cell polarization [82] or waves of actin polymerization [83] require

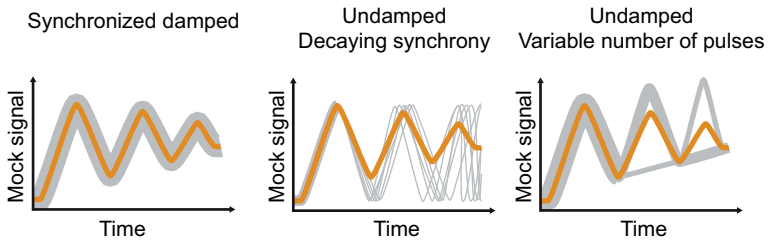

Figure 4.1: A hypothetical comparison between bulk and single cell measurements shows that identical results in bulk measurements might result from three completely different single cell scenarios. (a) A damped oscillation can be observed for the whole cell bulk, (b) the single cells exhibit undamped oscillation but with decaying synchrony or (c) fewer cells follow the oscillation with time [80, adapted from Fig. 3].

at least the combination of a negative and a positive feedback scheme.

In *D. discoideum*, many proteins are known to accumulate at the leading edge of the cell and therefore might participate in a positive actin polymerization enhancing feedback. Partially redundant pathways which simultaneously mediate chemotactic migration complicate the identification of key chemotactic response schemes, as redundant feedback systems can compensate for perturbed pathways [74]. Consequently, the experimental dissection of the signaling cascades underlying *D. discoideum* chemotaxis remains very challenging.

Precise and quick stimulation in combination with rapid monitoring of the intracellular protein distribution are necessary to detect alterations in the intrinsic time scales of the dynamic chemotactic response, caused by the depletion of distinct chemotactic pathways [81]. Intracellular protein distributions are monitored at high spatiotemporal resolution, but to precisely describe the chemotactic input-output relation, the resolution of the experimentally generated input has to be improved.

Even high spatiotemporal resolution in the observation of single cells does not guarantee an accurate description of cell response. Many publications have shown that cell-to-cell variability is ubiquitous. Cell manipulation, like gene transfection [84] or switching on the competence of bacteria to take up external DNA [85], is highly probabilistic and stochastic noise is already observed at the first steps of gene expression [7]. For complex signaling networks that rely on the interplay of dozens of proteins, an even higher variability in cell response has to be suspected.

Oudenarden et al., for example, proposes an preferred intracellular direction in gradient sensing [8]. If the inner feedback is aligned with the direction of the chemotactic gradient, a pronounced chemotactic response is observed, whereas if the inner feedback opposes the external gradient direction it possibly overrules the external stimulation. The cells exhibit a chemotactically induced polarization in the preferred direction of the intracellular feedback that potentially points away from the external concentration gradient. This effect results in a vastly heterogeneous response to a chemotactic stimulus within a population of genetically identical cells. However, a repeatedly stimulated single cell will show reproducible responses within tight error margins. Therefore, individual cell response cannot be taken as typical within a heterogeneous cell bulk. Accordingly broad statistical analysis is pivotal to reliably describe the chemotactic input-output relation, presuming the identical stimulation of entire cell ensembles.

While a broad statistical treatment clearly is necessary, analysis solely based on bulk behavior is also not ideally suited to fully describe the underlying principles of cellular feedback. A cell ensemble responding to an external stimulation by a synchronized damped oscillation (Fig. 4.1a) results in the same bulk measurement as either the same cell ensemble responding by an undamped oscillation but with decaying synchrony (Fig. 4.1b) or an undamped oscillation with less cells participating over time (Fig. 4.1c) [80]. A bulk measurement cannot thoroughly describe the underlying dynamics of the cell response. Consequently, full information is only ensured if a bulk of single cell measurements is statistically analyzed.

4.2 Ideal Chemotactic Stimuli

In conclusion, advancing the spatiotemporal resolution of the chemotactic input is only meaningful if the statistic analysis of the output is also improved, as well as the converse. Only if the average response with respect to a precisely known stimulus is accurately described, experimental results and theoretical descriptions can be meaningfully matched. Advanced experimental designs probing eukaryotic chemotaxis need to be able to expose entire cell ensembles to identical chemotactic stimulation that is repeatably and precisely tunable at the intrinsic time scales of the chemotactic

feedback. We find a ideal chemotactic stimulation to allow for:

- reproducible generation of homogeneous concentration gradients,
- repetitive stimulation of entire cell ensemble with identical chemotactic gradients
- rapid modification of the chemotactic gradient on the time scales of intracellular feedback.

Microfluidic designs addressing the chemotactic response of *D. discoideum* need to find a compromise in flow velocity which allows for the reproducible generation of homogeneous chemotactic gradients at low flow velocity without loosing the ability to rapidly tune the concentration gradients on time scales matching the inherent time scales of chemotactic feedback schemes at high flow velocity. The existing designs mostly focus on the generation of concentration gradients such as gradient mixing in labyrinth like structures or the creation of rapidly tunable perturbations as in flow photolysis experiments and the signal generator.

Furthermore, some of the presented designs create sophisticated chemotactic stimulation for individual cells like microsphere experiments but a thorough description of the chemotactic input-output relation also requires broad statistical analysis.

Part I

Generating Alternating Gradient Fields

Chapter 5

Chemotactic Gradient Generator

Significant improvements in the mathematical modeling of eukaryotic chemotaxis and the increasingly complex biochemical network found to control the chemotactic response in *D. discoideum*, have created the demand for new experimental assays. New setups need to reproducibly generate homogeneous concentration gradients, rapidly tune them in space and time and probe large enough cell ensembles for a reliable statistical analysis.

Here, I present the Chemotactic Gradient Generator (CGG) a microfluidic approach based on a double T-junction chamber. It allows for rapid manipulation of precisely shaped concentration gradients of chemoattractant that extend over several hundred microns. Diffusive broadening of the stream interfaces results in homogeneous concentration gradients, whereas hydrodynamic focusing of the individual streams facilitates fast positioning of the evolving concentration gradients.

In the following chapter, I establish the concentration distribution within the flow chamber by fluorescence measurements of the concentration distribution of the dye Fluorescein, and in collaboration with C. Weber, A. Zielinski and Prof. T. Franosch confirm the observed results by finite element calculation (FEC). The presented chemotactic gradient generator combines simultaneous exposure of several dozens of cells to identical chemotactic gradient fields, combining reproducible stimulation for all cells and rapid alteration of gradient direction at a maximal switching frequency of up to 0.7 Hz.

5.1 Concept of a Chemotactic Switch

The double T-junction chamber of the CGG consists of three separate inlets: a central, neutral flow (gray), and two side flows, containing the chemoattractant (red). Variable pressure application at the side flows enables sweeping of the streams from one side of the chamber to the other, thereby generating opposing gradient fields (t_1 to t_2 in Fig. 5.1).

At the start of the experiment, no chemotactic gradient is applied to the cells, which probe their surroundings by stochastic pseudopod extension (t_0, Fig. 5.1a). A controlled displacement of the stream interfaces exposes the cells to a chemotactic stimulus. The cells initiate directed migration into the direction of the chemotactic gradient and polarize for sufficiently long lasting stimuli (t_1, Fig. 5.1b). A further displacement of the stream interfaces, shifts the opposing stream boundary towards the cell ensemble, reversing the direction of the chemotactic gradient. The cells are forced to adjust to the new stimulus and re-polarize in the new direction (t_2, Fig. 5.1c). In order to generate this response, the cells need to iteratively adapt their actin polymerization activity allowing for systematic investigation of the chemotactic process.

5.2 3 inlet Double T-Junction Flow Chamber

In our setup, we use 'µ-slide 3in1' microfluidic chambers (Ibidi, Munich, Germany) with three $0.4x1.0\,\mathrm{mm}^2$ inflows that converge under an angle of $\alpha = 32°$ to the main channel of dimensions $0.4x3.0x23.7\,\mathrm{mm}^3$ (Fig. 5.2). Both side flows (SF) are connected to reservoirs, built from two 20 ml syringes (Braun Melsungen AG, Melsungen, Germany), separately connected to a customized 'Suction Control' pressure pump (Nanion, Munich, Germany). Two micrometer valves (Upchurch Scientific, Oak Harbor, WA, USA) reduce the flow velocities at the SFs and allow for precise adjustment of the inflow velocities applied to the side inflows. The central flow (CF) is connected to an 'Infusion' syringe pump (TSE Systems, Bad Homburg, Germany), which generates a stable flow of 1 ml/h. Measurements are performed with an Axiovert 135 TV microscope (Zeiss, Oberkochen, Germany), with LD Plan-Neofluar objectives of 20 x / 0.50 N.A. and 40 x / 0.75 N.A.

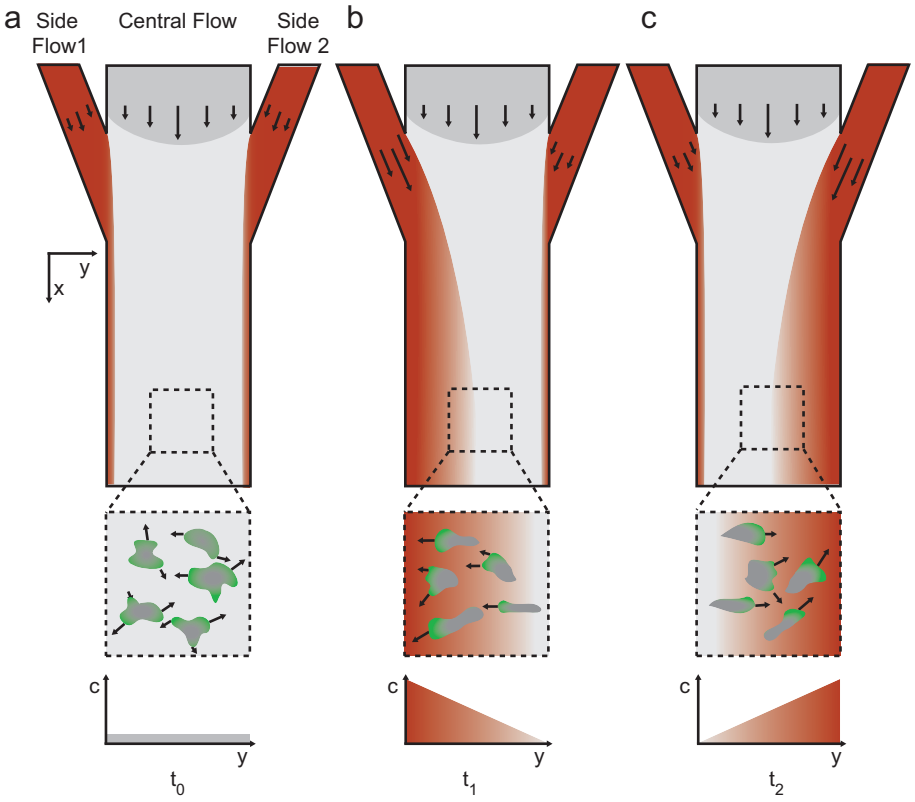

Figure 5.1: Concept of a microfluidic, chemotactic gradient generator [86]: (a) At t_0, no chemoattractant (red) is introduced to the cell site (dashed box). Cells form random protrusions, as indicated in green, representing actin polymerization. The chemoattractant concentration is constant at level zero within the cell observation area. The coordinate system is given by the x-axis, pointing in flow direction, the y-axis perpendicular to the flow, and the z-axis perpendicular to the plane of drawing. (b) At t_1, side flow 1 (SF1) introduces a chemotactic stimulus to the cell ensemble, leading to directed cell migration of the cells in gradient direction to the left. (c) At t_2, the chemotactic stimulus is switched to side flow 2 (SF2), reversing gradient direction. The cells are forced to switch polarization to migrate in the opposite direction, now to the right.

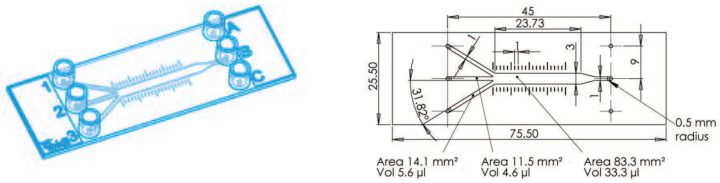

Figure 5.2: In the presented experiments uncoated µslides 3inI from Ibidi are used. The relatively large microfluidic channels of $0.4x3.0x23.7\,\mathrm{mm}^3$, facilitate low flow velocities and a uniform velocity distribution at the cell side.

magnification (Zeiss, Oberkochen, Germany) in combination with a DV2 DualView system (Photometrics, Tucson, AZ, USA). The dual view system allows for simultaneous observation of cells with a Lim-Gfp label and the fluorescent dye Alexa 568, used to mimic the concentration distribution of cAMP (also see Appendix for Material & Methods and Fig. 5.3).

5.3 How Gradients Emerge in the Flow Chamber

The first step towards an accurate investigation of eukaryotic chemotaxis is the controlled generation of homogeneous concentration gradients. In the presented setup, the gradients directly evolve in the flow chamber. The microfluidic T-junction has been introduced by Kamholz et al. to determine the diffusion of soluble dyes [87, 88]. In a laminar flow, two merging streams stay separate and no immediate mixing occurs. Yet, diffusion of soluble analytics takes place at the stream interface [89] and an inter-diffusive region, where both streams mix, emerges.

Since the concentration gradients are generated by diffusive broadening within the flow chamber, flow velocity largely influences the shape and extension of the concentration gradients. Regions with large flow velocities result in steeper gradients and a less extended inter-diffusive region as less time is available for diffusion.

Flow in a rectangular duct

The velocity profile of a rectangular duct obtained by finite element calculation (FEC) is plotted in Fig. 5.4a. For typical inflow volumes given in later

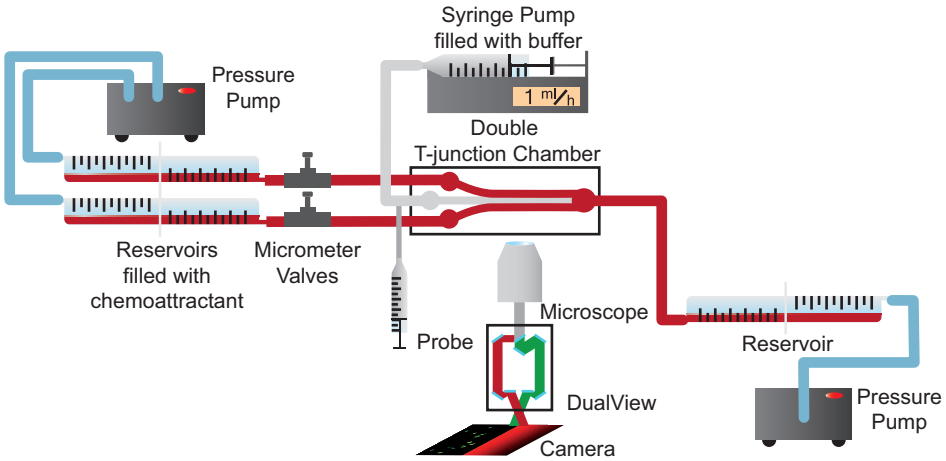

Figure 5.3: Schematic drawing of the Chemotactic Gradient Generator (CGG). The GCC is based on a double T-junction microfluidic chamber. A combination of a syringe pump connected to the middle inlet and two pneumatic pressure pumps attached to both outer inlets and the outlet of the flow chamber facilitate accurate control of the flow velocities applied to the individual inlets. Micrometer valves are added to the setup to increase the flow resistance at the outer inlets. An increased flow resistance allows for a larger pressure difference during gradient switching, minimizing the sensitivity of the chemotactic gradients to the pressure tolerance of the pneumatic pumps. A DualView imaging system attached to the microscope enables parallel imaging of two fluorescence channels, allowing for the simultaneous measurement of concentration gradients and living cells.

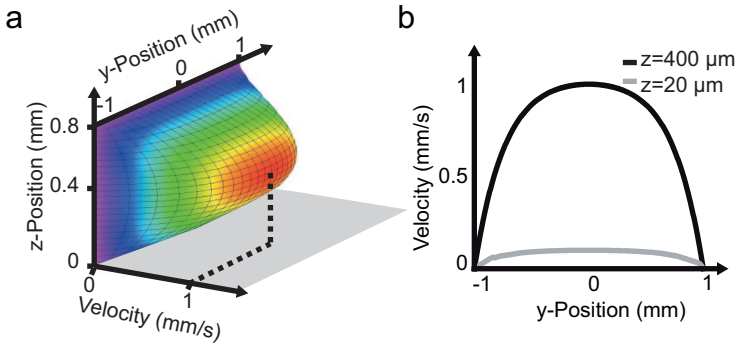

Figure 5.4: Flow profile of a rectangular duct. (a) FECs for a typical experimental obtained flow velocity in a rectangular duct $0.8x2\,\mathrm{mm}^2$ yield the expected parabolic velocity distribution with its maximum flow speed at the center of the duct and vanishing flow at the side walls. (b) A closer look at the flow profile shows a more uniform velocity distribution at $z = 20\,\mu\mathrm{m}$ (gray), where the investigated cells adhere in live cell experiments, when compared to the pronounced parabolic flow profile that is found at $z = 400\,\mu\mathrm{m}$ (black). The homogeneous flow profile close to the chamber bottom, $z = 20\,\mu\mathrm{m}$, facilitates that all investigated cells are subjected to comparable concentration gradients.

live cell measurements and a height of the rectangular duct of $z = 800\,\mu\mathrm{m}$, FECs yield a flow velocity of $1\,\mathrm{mm/s}$ and a distinct parabolic flow profile at the center of the flow,$z = 400\,\mu\mathrm{m}$ (Fig. 5.4b, black curve). In later live cell experiments, the cells adhere to the chamber bottom. Here, at $z = 20\,\mu\mathrm{m}$, the flow velocity is reduced to only $1\,\mu\mathrm{m/s}$ and a much more uniform velocity distribution is observed (Fig. 5.4b, gray curve). Even when the stream interfaces are swept perpendicular to the flow direction, the flow velocity is only changed slightly, allowing for the generation of homogeneous chemotactic gradients. The low flow velocities further result in an extended inter-diffusive region and therefore concentration gradients that extend over several hundred microns.

Generation of homogeneous concentration gradients with variable steepness

The position downstream the flow chamber defines the gradient shape in the same way as the overall flow velocity. Further downstream, more time has elapsed and a broader inter-diffusive region emerges. Consequentially, we find steeper concentration gradients close to the merging point of the three streams as compared to the concentration gradients observed close to

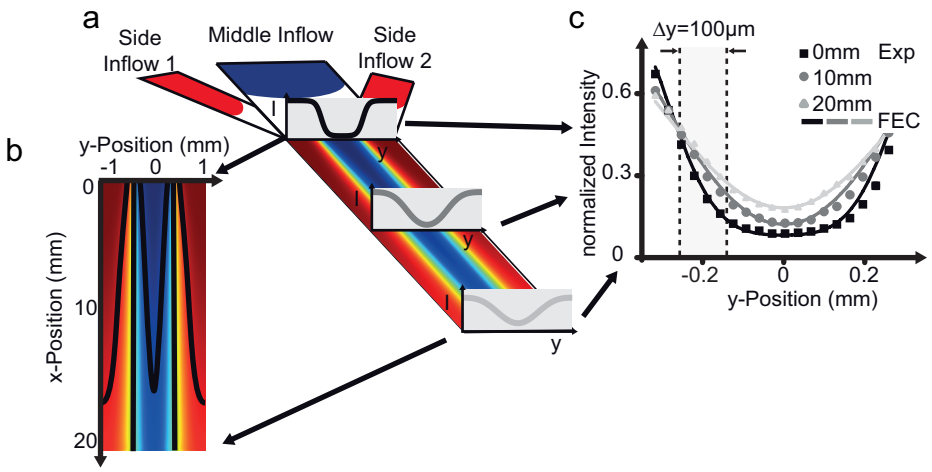

Figure 5.5: FECs show the generation of homogeneous gradients at the flow interfaces by diffusive broadening. (a) The three streams at 1 (red) and 0 (blue) concentration of a soluble analytic or fluorescent dye meet at the merging point of the flow chamber, $x = 0\,\text{mm}$. As diffusion takes place the stream interfaces broaden as indicated by the three concentration profiles at $x = 0$, 10, 20 mm. (b) Iso-concentration lines at concentrations of 0.3, 0.5 and 0.7 (black lines) illustrate a reduction of gradient steepness downstream in the flow chamber. At $x = 0\,\text{mm}$ the iso-concentration lines are in close proximity yielding steep concentration gradients, whereas the high and low concentrations vanish downstream, resulting in more shallow gradients. (c) Comparison of fluorescence measurements of the concentration distribution of Fluorescein and FECs at $x = 0$, 10, 20 mm. FECs and fluorescence measurements are found in excellent agreement, ranging from 15% to 40% reduction of the concentration over 100 µm, for the flow velocities typically used in our live cell experiments.

the chamber outlet.

To determine the actual distribution of concentration gradients in our flow chamber, we performed fluorescence measurements with the fluorescent dye Fluorescein and further FECs. Due to the similar diffusion coefficients of cAMP and Fluorescein [90], Fluorescein is ideally suited to mimic how the concentration gradients of cAMP emerge in the flow chamber during later live cell experiments.

Diffusion starts as soon as the three streams merge at the main channel of the flow chamber (Fig. 5.5a, $x = 0\,\text{mm}$). FECs with a normalized concentration of 1 (red) at the outer inlets and a concentration of 0 (blue) at the inner inlet of the flow chamber illustrate this effect. At the beginning of the chamber, steep concentration gradients are found (black curve in Fig. 5.5a) that become increasingly shallow downstream in the microfluidic chamber ($x = 10\,\text{mm}$ and $x = 20\,\text{mm}$, dark gray and light gray curves in Fig. 5.5a). A concentration map of the main channel, shows iso-concentration lines at 0.3, 0.5 and 0.7 percent of the maximal concentration. At $x = 0$ all three iso-concentration lines are found in close proximity, representing a steep concentration gradient. At $x = 20\,\text{mm}$ the concentration gradient is considerably reduced and no concentrations as high as 0.7 or as low as 0.3 are observed anymore (Fig. 5.5b). The concentration gradients found in FECs are in excellent agreement with experimentally obtained concentration profiles off the main channel (Fig. 5.5c). Fluorescence measurements and FECs indicate a decrease in chemoattractant concentration over a width of $100\,\mu\text{m}$, ranging from 15% to 40% off the maximal concentration, for typical flow velocities used in the experiments of this thesis (Fig. 5.5c, gray box).

The variety of different gradient steepnesses generated in our setup is comparable to the distribution of chemotactic gradients achieved in micropipette assays. Nevertheless, the concentration gradients that emerge in our flow chamber feature an extended, homogeneous region, allowing for repeated exposure of entire cell ensembles to identical stimuli, whereas micropipette experiments suffer from inhomogeneous gradient distributions and a rising background in chemoattractant concentration over time. The steady flow in our flow chamber facilitates unmodified chemotactic gradients over the course of a several hour experiment, promoting precisely reproducible measurements.

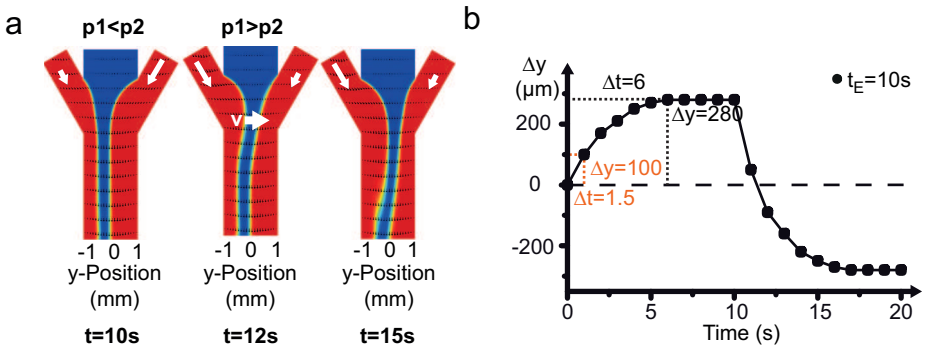

Figure 5.6: Theoretical lower limit for transition times between gradient fields of opposing directions. (a) FECs for alternating gradients with an exposure time of $t_E = 10\,s$. The displacement of the stream interfaces solely depends on the inflow speeds of the side inflows (white arrow at $t = 12\,s$). Gradient switching propagates down the flow chamber with the flow velocity of the main channel $\mathbf{v}$ (white arrow at $t = 15\,s$). (b) FECs yield a transition time of $t = 6\,s$ for a full displacement of the gradient across $y = 280\,\mu m$. In live cell experiments, a displacement of $y = 100\,\mu m$ is sufficient, still over-spanning several cell length, resulting in a lower theoretical limit of $t = 6\,s$ for the transition time (orange dotted line). The rapid transition time achievable in our setup allows for gradient manipulation at the intrinsic time scales of the cells' chemotactic response.

5.4 Rapid manipulation of gradient direction

Homogeneous gradients and long-term stability in the CGG lay the ground for a reliable description of the chemotactic response, but systematic investigation in response to changing gradient direction demands rapid manipulation of the gradient direction. The three inlet design of the CGG enables precise adjustment of the flow speeds applied to each of the three inflows, facilitating accurate modification of width and position of the individual streams. Symmetrically increasing the flow speed of the outer inlets reduces the width of the middle stream, called hydrodynamic focusing [91]. Asymmetric pressure application to both outer inlets shifts the stream in the direction of the low pressure inlet (Fig. 5.6a).

Accurate positioning of the gradients

In our setup, reproducible gradient switching is enabled by a syringe pump applying a constant flow rate of $1\,^{ml}/_{h}$ to the middle inlet, therefore ensuring a stable mid stream, and two pressure pumps facilitating rapid changes of

the inflow velocities at the outer inlets. The large volume of the double T-junction chamber used in the CGG results in a small flow resistance of the microfluidic setup and therefore a pronounced sensitivity of the flow velocities to instabilities of the pneumatic pressure pumps with a tolerance of 0.5 mbar. Insertion of additional microfluidic valves in front of the outer inlets of the flow chamber yields the possibility to adjust the flow resistance to the pressure range of the used pumps. The pressure difference during gradient switching experiments is increased to approximately 50 mbar, reducing the effect of pressure instabilities on position and shape of the chemotactic gradient, thereby allowing for sound positioning of the concentration gradients in the vicinity of the investigated cell ensemble. As small pressure variations have a large effect on the chemotactic gradients, changes in the atmospheric pressure during the experiment will also reduce gradient stability. Therefore, I added an additional pressure pump to the outlet of the flow chamber to further increase the long-term stability of the experiment.

Theoretical limit of the transition time

The flow speed applied to the outer inlets determines how fast the stream interfaces are swept perpendicular to the flow direction in the main chamber (Fig. 5.6a, white arrow at $t = 10\,\mathrm{s}$) [79]. For flow velocities typical to our measurements and a stream displacement perpendicular to the flow direction of $\Delta y = 280\,\mu\mathrm{m}$, we find a transition time of approximately 6 s. However, if faster transition times are necessary, a displacement of $\Delta y = 100\,\mu\mathrm{m}$, still spanning over several cell lengths, would be sufficient, resulting in a lower limit of the transition time of 1.5 s, meaning a maximum switching frequency of 0.7 Hz (Fig. 5.6b) .

Long-term stability

The fluorescence measurement in Fig. 5.7 shows a switching process for a measurement with an exposure time of $t_\mathrm{E} = 600\,\mathrm{s}$. The exposure time is defined as the timespan between the initiation of two consecutive switches. In Fig. 5.7, the switch is initiated at $t = 0\,\mathrm{s}$ (Fig. 5.7b, red curve) and a stable concentration distribution is again observed after 12 s (Fig. 5.7b, blue curve). While it takes some time for the gradients to reach a constant value (Fig, 5.7b, green curve), an actual switch in the direction of the gradient is

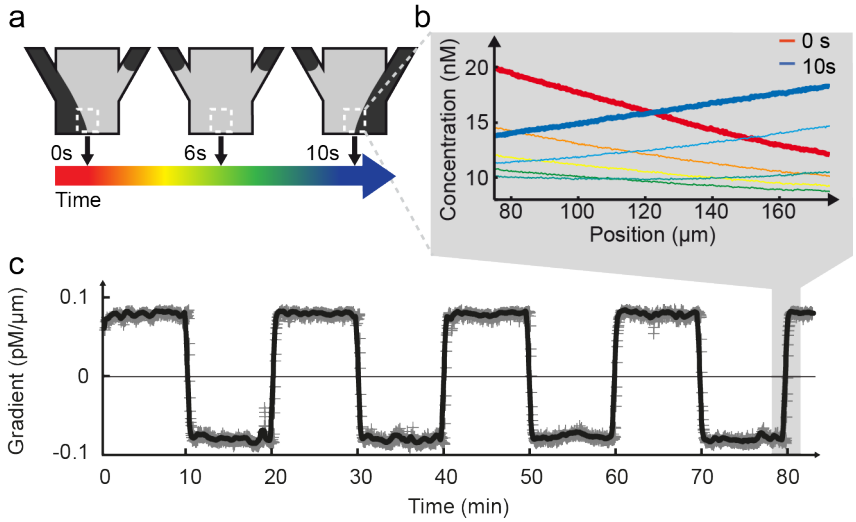

Figure 5.7: Fluorescence measurement of the transition between two opposing gradient fields. (a) Schematic view of the switching process, as indicated by the color bar, from $t = 0\,\mathrm{s}$ (red) to $t = 12\,\mathrm{s}$ (blue) used for the fluorescence measurement in b). (b) Fluorescence measurement illustrating the transition process between two opposing gradient directions. The entire transition takes 12 s but the actual reversing of gradient direction happens within one frame (2 s) (c) Stability of the concentration gradients during 8 consecutive switches in gradient direction. The running average over 10 s (black curve) and the single measurements are plotted over the time span of 8 switches for a switching period of 10 min. A high stability of the gradient steepness is achieved with a variance for each 10 min period below 5 % in gradient steepness.

fulfilled within one frame (2 s). The gradient steepness increases afterward but the investigated cells are already exposed to a gradient in the opposing direction. The gradient remains stable over an 80 min experiment and the first switch is within tight error margins of less than 5% when compared to the previous (Fig. 5.7c).

Overall, our microfluidic setup facilitates reliable application of time-varying, homogeneous bidirectional gradient fields, which thus enables us to reliably probe the re-polarization behavior of chemotactic cells in response to alternating gradients. We find the flow speeds used in our experiments to be a great compromise, allowing for the generation of homogeneous gradients by diffusion without loosing the ability to rapidly manipulate the gradient direction.

5.5 Flow effects on living cells

Reproducible gradient switching in our flow chamber is enabled by a steady laminar flow. Yet, undesirable effects such as shear-induced gene expression [92, 93] and reduction of the chemotactic gradient by the cells [94] are reported to impair live cell measurements in microfluidic devices.

Shear stress induced migration

Many cells types respond to shear stress as it is exerted by the steady flow in a microfluidic chamber. Depending on the shear rate, endothelial cells align their stress fibers [95] and the gene regulation is altered [96]. In *D. discoideum*, Decave et al. found a shear stress induced migration [97]. The cells align their migration with the flow direction starting at 0.7 Pa. In our live cell experiments, the low flow speed of only 100 µm/s produces a shear rate of less than 1% of this critical shear stress [97].

Flow perturbation by the cells

High flow speeds further cause flow perturbations generated by the cells themselves that reduce an applied chemoattractant gradient, as has been shown by Beta et al. [94]. A concentration gradient approaching a spherical obstacle is split, yielding the same concentration around its entire perimeter,

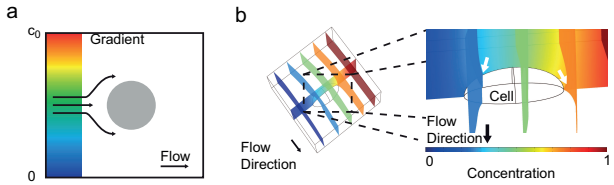

Figure 5.8: Flow perturbation by cells in microfluidic devices. (a) An obstacle splits the laminar flow, so that the wedding layer originates in one point. The concentration gradient is lost but will quickly rebuilt by diffusion [94, adapted from Fig. 2]. The degree of gradient reduction over the cell depends on flow speed, cell size and cell orientation up to the point were most of the gradient is lost. (b) We repeat the FECs by Beta et al. to determine the grade of gradient reduction in our setup. We find that the iso.concentration lines (red to blue) are not deformed on the first sight. A closer look reveals slight deviation at the cell's surface (white arrows). Overall, FECs only show insignificant gradient reduction for our experimental setting.

as the wetting layer originates in one point (Fig. 5.8a). However, due to diffusion, the gradient will build up again depending on the flow velocity. We repeated the FECs performed by Beta et al. to determine the degree of gradient reduction expected for our experimental conditions [94]. At first sight, no relevant bending of the iso-concentration planes is observed for a hypothetical cell in our experiment (Fig. 5.8b). A closer look reveals a slight perturbation of the chemotactic gradient at the cell's surface (white arrows in Fig. 5.8a). Yet, the small perturbation of the gradient profile across the hypothetical cell illustrates that gradient reduction at high flow velocities can be neglected in our experimental design.

Part II

Cell Response to Alternating Gradient Fields

Chapter 6

Chemotactic Timescales as observed in "Chemotactically Trapped" Cells

In the following, we prove the capability of our setup to initiate chemotactically induced oscillatory runs of *D. discoideum* cells at exposure times of $t_E = 600\,\mathrm{s}$. Subsequent experiments, gradually decreasing the exposure time to $t_E = 10\,\mathrm{s}$, result in a "chemotactically trapped" cell state, separating the process of directional sensing.

Oscillatory runs at long exposure times

In a first step, we excite chemotactically biased migration in living cells for exposure times of $t_E = 600\,\mathrm{s}$. The exposure time is defined as the period between the initiation of two switching events. Long gradient exposure times of $t_E = 600\,\mathrm{s}$, ensure that the cells are able to fully adjust their direction of locomotion and migrate in the direction of the new stimulus. The cells are monitored using the DualView technique. DualView facilitates simultaneous imaging of two fluorescence channels by displaying two images side by side on the CCD camera (Fig. 6.1a). For all fluorescence experiments, cells with a Gfp label are monitored in the green channel, whereas the concentration distribution within the observation region is visualized in the red channel using the fluorescent dye Alexa 568. Cell migration is traced by the ImageJ plugin CellEvaluator [98]. CellEvaluator assigns individual pixels

to cell clusters based on an intensity threshold and enables tracing of a cell cluster throughout a stack of images. In the following, the displacement of the cell's center of mass is analyzed. The cell's center of mass is defined for a homogeneous mass distribution of the cell's projection into the two dimensional plane of the microscope.

Fig. 6.1b illustrates the displacement of 7 cells (gray lines) parallel to the axis of gradient switching (y-direction). The cells migrate in the direction of the recent stimulus after the gradient direction (red line) is switched. The ensemble response is rather inhomogeneous but the averaged displacement (solid black line) indicates a clear bias of the migration direction in the direction of the chemotactic gradient $2-3\,\mathrm{min}$ after the gradient switch is initiated (dotted lines).

Although, starvation is initiated at the same time for all cells and all cells are subjected to the identical alternating chemotactic gradient field, a large variability of the chemotactically induced migratory response is observed for the individual tracks of 7 cells in the x-y-plane (Fig. 6.1c). Some cells clearly migrate in the direction of the chemotactic gradient gaining up to $100\,\mu\mathrm{m}$ in the direction of the recent gradient (white arrows), whereas other cells actually exhibit an overall displacement in the opposite direction (blue arrows).

These findings were to be expected based on results of Oudenardeen et al. [8], however, the observed heterogeneous cell response underlines the need for a critical and conscientious statistical analysis of the input-output relations found in live cell experiments.

Decreasing the exposure time leads to a "chemotactically trapped" cell state

Switching the chemotactic gradient direction with an exposure time of $t_E = 600\,\mathrm{s}$ showed that on average the cells follow the chemotactic stimulus by oscillatory runs. However, it is also observed that the cells expierence a delay before they adjust to the new gradient direction. Decreasing the exposure time should therefore impede the cells ability to follow the chemotactic gradient by migration.

We gradually decrease the exposure time from $t_E = 300\,\mathrm{s}$ to $t_E = 10\,\mathrm{s}$ and analyze the migration velocity $\mathbf{v}$ and the migration angle φ for 410

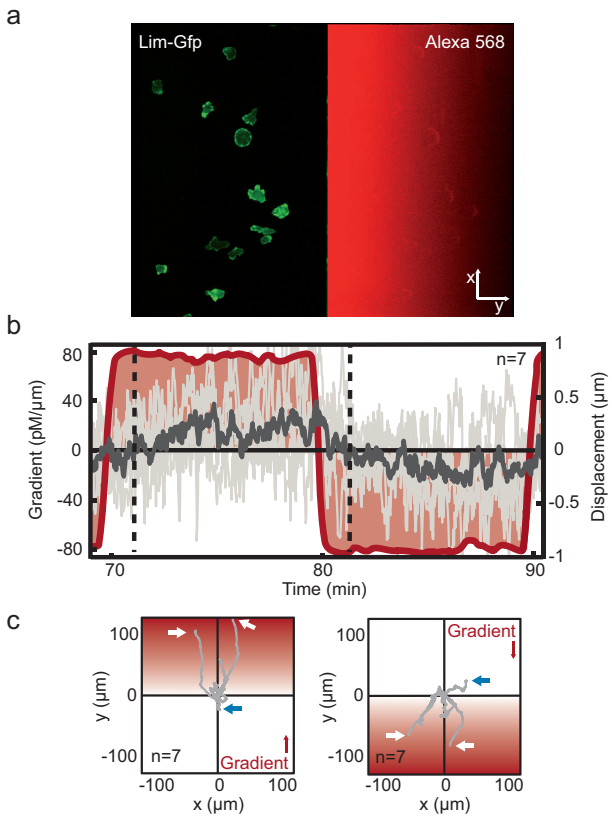

Figure 6.1: Oscillatory runs in response to alternating gradient directions. (a) Colored DualView image illustrating the simultaneous observation of the intensity distribution of Alexa 568 (red), mimicking the concentration distribution of cAMP and cells with a LimEΔcc-Gfp label (green). (b) The displacement of 7 cells (gray lines) in the direction of the chemotactic gradient (red line) results in an averaged bias of the migration direction in the direction of the chemotactic gradient (black line). We observe a response delay of approximately 3 min before the cells fully adjust to the altered gradient direction (dotted lines) (c) The individual cell trajectories in the x-y-plane with the position of the cell set to the origin when the gradient is switched show cells that are highly responsive to the chemotactic stimulation and gain up to 100 µm in the direction of the chemotactic gradient during one switching period (white arrows). Other cells hardly migrate in the direction of the stimulus or even migrate in the opposing direction (blue arrows).

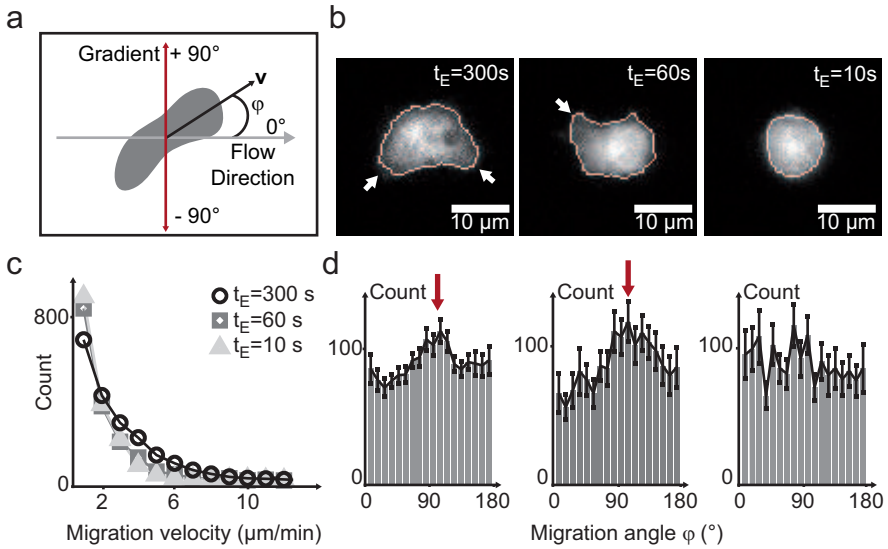

Figure 6.2: Gradual decrease in gradient exposure time (from $t_E = 300\,\mathrm{s}$ to $t_E = 10\,\mathrm{s}$) leads to "chemotactically trapped" cells. (a) Center of mass motion of migrating cells is analyzed in terms of migration velocity $\mathbf{v}$ and migration angle φ with respect to the flow direction, entailing the direction of the chemotactic gradient at $\varphi = |\pm 90°|$. (b) For chemotactic gradient exposure times of $t_E = 300\,\mathrm{s}$, cells show directed pseudopod formation (arrows, left). For shorter exposure times of $t_E = 60\,\mathrm{s}$, pseudopod extension is less pronounced (arrow, center) and for the most rapid switching ($t_E = 10\,\mathrm{s}$) cells round up and pseudopod formation is absent (right). (c) Motion analysis for 410 switching events out of 42 cells with free-Gfp label reveals a decrease in migration velocities for exposure times of $t_E = 60\,\mathrm{s}$ and $t_E = 10\,\mathrm{s}$ while for an exposure time of $t_E = 300\,\mathrm{s}$, a large number of cells exhibits migration velocities above $6\,\mu\mathrm{m}/\mathrm{min}$. (d) Analysis of the cellular migration yields distinct peaks in the direction of the chemotactic gradients at $\varphi = |\pm 90°|$ for exposure times of $t_E = 300\,\mathrm{s}$ and $t_E = 60\,\mathrm{s}$ (red arrow), while a nearly uniform angle distribution is observed for rapid switching with $t_E = 10\,\mathrm{s}$, indicating a 'chemotactically trapped' cell state, where cells cannot follow the fast gradient switching due to slower internal re-polarization times [86].

switching events from a total of 42 cells (Fig. 6.2a). At first sight, the cells form pronounced pseudopods in the direction of the gradient for an exposure time of $t_E = 300\,\mathrm{s}$ (white arrow in Fig. 6.2b, left). For a moderate exposure time of $t_E = 60\,\mathrm{s}$, the pseudopodia are less pronounced and the cells show a rounder cell perimeter (white arrow in Fig. 6.2b, center), whereas for an exposure time of $t_E = 10\,\mathrm{s}$ the displayed cell completely rounds up (Fig. 6.2b, right).

Analysis of migration velocity $\mathbf{v}$ and migration angle φ support this observation. For the long exposure time of $t_E = 300\,\mathrm{s}$, the distribution of the migration velocity yields more cells at velocities above 4 µm/min (black circles in Fig. 6.2c) as for an exposure time of $t_E = 60\,\mathrm{s}$ and $t_E = 10\,\mathrm{s}$. Furthermore, the migration angle distribution shows a peak in the direction of the alternating gradients at $\varphi = |\pm 90°|$ (red arrow in Fig. 6.2c, left). Large migration velocities and a bias of the migration angle represent oscillatory migration in the axis of gradient switching at long exposure times.

For a moderate exposure time of $t_E = 60\,\mathrm{s}$, the angle distribution also shows a distinct peak at $\varphi = |\pm 90°|$ (red arrow in Fig. 6.2d, center). However, at $t_E = 60\,\mathrm{s}$ a lack of high migration velocities is noticed when compared to s (gray squares in Fig. 6.2c). We assume that for an exposure time of $t_E = 60\,\mathrm{s}$ the cells start to extend pseudopods in the direction of the recent gradient, resulting in a bias of the migration angle, but the gradient is switched before the cell actually initiates migration.

At an exposure time of $t_E = 10\,\mathrm{s}$, a round cell perimeter, no significantly large migration velocities (gray triangles in Fig. 6.2c) and a uniform distribution of the migration angles (Fig. 6.2d, right) are observed. We refer to this cell state as "chemotactically trapped" cells. The cells recognize the gradient but intracellular feedback seems too slow to modify cell migration before gradient direction is switched again.

Separation of directional sensing at high switching frequencies

In the "chemotactically trapped" cell state, the cells exhibit a round cell perimeter. Rounded up *D. discoideum* cells are also observed after a uniform increase in the concentration of chemoattractant [54]. However, cells that are subjected to a pulse of chemoattractant adapt to the increased con-

centration and quickly regain a regular unbiased migration. Here, we find the cells "trapped" over a long time period. This cell response can not be interpreted in a way by which the cells sense a uniform concentration distribution. Instead the cells have to actually resolve the direction of gradient switching even at the fast exposure time of $t_E = 10\,\mathrm{s}$.

The timescales found in our experiment agree with previously reported chemotactic response dynamics. Chen et al. used cells that had been fixed and fluorescently stained at various time points after addition of cAMP. They observed two peaks of F-actin polymerization in response to a uniform increase in cAMP concentration [54]. The first peak is monitored within the first 10 s after cAMP has been added to the cells and a second much broader but less pronounced peak is found after roughly 1 min. Both peaks of F-actin polymerization can be connected to the single steps of the chemotactic response of directional sensing and migration.

We find that the cells are still able to recognize the direction of the chemotactic gradient for an exposure time of $t_E = 10\,\mathrm{s}$ and that first pseudopods are extended for an exposure time of $t_E = 60\,\mathrm{s}$. We conclude that the CGG is capable of exciting the three chemotactic steps of directional sensing, migration and cell polarization. The formation of new pseudopods in response to chemotactic stimulation is observed at an exposure time of $t_E = 60\,\mathrm{s}$ and cellular polarization takes place for longer lasting stimuli in migrating cells. At an exposure time of $t_E = 10\,\mathrm{s}$, the process of directional sensing is investigated without the need of drastic perturbation of the cells, such as the de-polymerization of the actin cortex by Latrunculin [99]. We, for the first time, present an experimental approach that is capable of the stimulation of living cells with alternating homogenous chemotactic gradients at the intrinsic time scales of individual regulatory networks of the chemotactic response. Yet, further investigation need to be done to monitor the intracellular distribution of specific signaling molecules, such as PI3-Kinase, promising a better understanding of directional sensing.

Chapter 7

Two Types of Migratory Response

The heterogeneous cell response of seemingly highly responsive and less responsive cells, observed for oscillatory runs at long exposure times, emerges from fundamentally different migratory behavior (see Fig. 2.5). The first migration type is observed in micropipette assays, if the micropipette is brought close to the cell [76]. The steep chemotactic gradient at the micropipette tip stimulates accumulation of PI3-Kinase, eventually leading to the formation of a fresh pseudopod. In contrast, cells located further away from the tip experience a shallow chemotactic gradient and are more likely to keep their leading edge. Cells in shallow gradients favor to turn like a car, adjusting to the direction of the chemotactic gradient by Phospholipase A2 (PlA2) mediated, splitting of the leading edge. Theoretical models nicely explain the one or the other migratory response but deeper insight into which migratory response is favored in dependence of gradient shape and developmental stage of the cells is still missing (also see section 2.3).

In the following I present analysis methods to distinguish between the two migratory behavior. We introduce a fluorescence distribution moment (FDM) to quantify intracellular actin polymerization dynamics in repolymerizing cells (Section 7.2), and the migration angle φ to quantify the migratory response of stably polarized cells (Section 7.3). Both analysis methods lead the way to an automatized investigation of the chemotactic cell response of entire cell ensembles, mandatory for an objective classification of chemotactic feedback in *D. discoideum*. It further turns out that cell

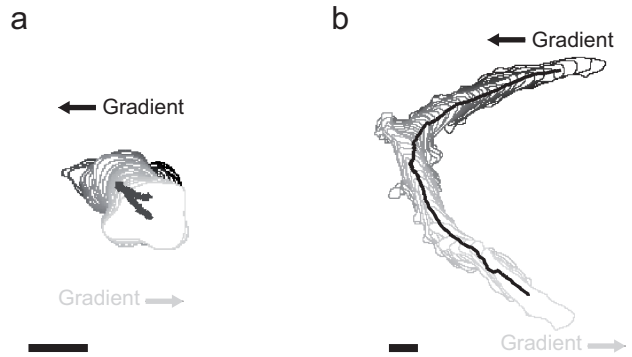

Figure 7.1: Two types of migratory response are observed after a switch in gradient direction. (a) The cells of the first migration type re-polymerize their actin cortex in response to a switch in the direction of the gradient. The cells form new pseudopods, the rear of the cell becomes the new leading edge and the former leading edge becomes the new rear. During the re-polymerization process almost no migration is observed. (b) The cells of the second migration type keep a stable leading edge. They perform an "U-Turn". The cells are elongated and migrate relatively fast due to a stable polarization in actin polymerization. The scale bars are 10 µm. Cell outlines are plotted every 30 s from black to light gray.

shape quantified by the eccentricity of an ellipse fitted to the cell perimeter is best suited to monitor the ratio of cells that exhibit the first or the second migration type.

7.1 Characteristics of *Dictyostelium discoideum* Migration

Amoeboid migration in the absence of external cues, can be separated into two different parts. Diffusion like parts, where the cell reorients its migration direction, are disrupted by phases of persistent migration, referred to as Levi flights [100].

Both phases of amoeboid migration feature a specific pattern of pseudopod formation. Bosgraf et al. distinguish two types of pseudopods, called de novo and splitting pseudopod [101]. A de novo pseudopod forms independently of the direction of the previously formed pseudopod, whereas a split pseudopod, splits off at the preceding pseudopod, conserving its direction. Cells tend to form de novo pseudopods during the phases of diffusion like migration. During phases of persistent migration, cells exhibit a sponta-

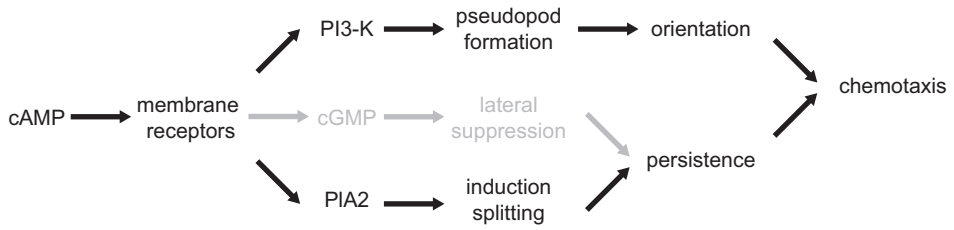

Figure 7.2: PI3-Kinase and PlA2 mediate Chemotaxis in *D. discoideum* (adapted from [40]). Bosgraf et al. propose the two pathways of PI3-Kinase induced formation of fresh pseudopods and PlA2 induced splitting of the leading edge to respectively mediate cell orientation and persistent migration. A third pathway, based on the signaling molecule cGMP, suppresses lateral pseudopodia (gray).

neous intracellular polarization featuring a stable leading edge, where split pseudopods emerge.

On the molecular basis of both migratory behavior, PI3-Kinase based formation of pseudopods has already been introduced as intracellular mediator of the chemotactic compass (section 2.2). One protein supposed to mediate persistent migration by the splitting of the leading edge is Phospholipase A2 (PlA2). Yet, the molecular mechanism of PlA2 mediated chemotaxis is still widely unknown [102].

Migratory response to chemotactic stimulation

If now a chemotactic stimulation is applied, cell migration has to align with the direction of the chemotactic gradient. The formation of fresh pseudopods results in a fast alignment with the external stimulus. Yet, constant reorientation of the cell, can also quickly defer the cell. In contrast, a cell that migrates with a large degree of persistence, can only slowly redirect its migration in the direction of the chemotactic stimulus. Still, once aligned with the external stimulation, the cell stays on track.

However experimental investigation, demonstrates that inhibiting single signaling pathways will generally not stop directed migration [103]. Yet, simultaneous blocking PI3-Kinase and PlA2 severely compromises the chemotactic response [75], resulting in a model of parallel pathways, that is completed by cGMP signaling at the uropod (Fig. 7.2). Bosgraf et al. propose that PI3-Kinase based formation of de novo pseudopods results in an enhanced orientation of the cell, whereas the PlA2 induced splitting of the

leading edge results in a more persistent migration [40, 78].

Bosgraf et al used cells that accidentally lost track of the chemotactic gradient and analyzed their way back. Yet, to gain deeper insight on how the single parallel pathways are promoted by environmental conditions like gradient steepness or the ongoing starvation of the cells, a more systematic experimental approach is needed. Our setup facilitates stimulation with repetitively reversed gradient direction and exposure of entire cell ensembles to exactly the same initial conditions. The CGG lays the ground for a systematic and quantitative analysis of chemotactic migration.

Actin polymerization marker: the fusion-protein LimEΔcc-Gfp

The polymerization of actin is a critical step in the formation of most cell protrusions and therefore a suitable indicator to distinguish between the formation of fresh pseudopods or a constant leading edge. Several fusion proteins can possibly be used to visualize actin structures within the cell. The most obvious are fluorescently tagged actin oligomeres [104]. However, these are embedded into the actin network and will therefore mark already existing actin structure the same way than newly evolving cell protrusions. In contrast, the LimEΔcc protein promotes actin polymerization but is not included into the actin structure [105]. Therefore a fusion protein of LimEΔcc and Gfp allows for the monitoring of freshly polymerized actin and discriminates established actin structures like the cell cortex. We use the LimEΔcc-Gfp label as a marker of the actin polymerization dynamics in all of the following measurements.

7.2 Re-polymerizing Cells

The first migration type is defined by cells that form fresh pseudopods in the direction of the chemotactic gradient (Fig. 7.1, left). A change in the direction of the chemotactic gradient, initiates a re-polymerization process of the cell and the cell forms new pseudopods at its former rear. Constant re-polymerization of the cell cortex prevent the formation of a stable intracellular polarization.

To quantitatively describe the re-polymerization process in these transiently polarized cells, we introduce the fluorescence distribution moment

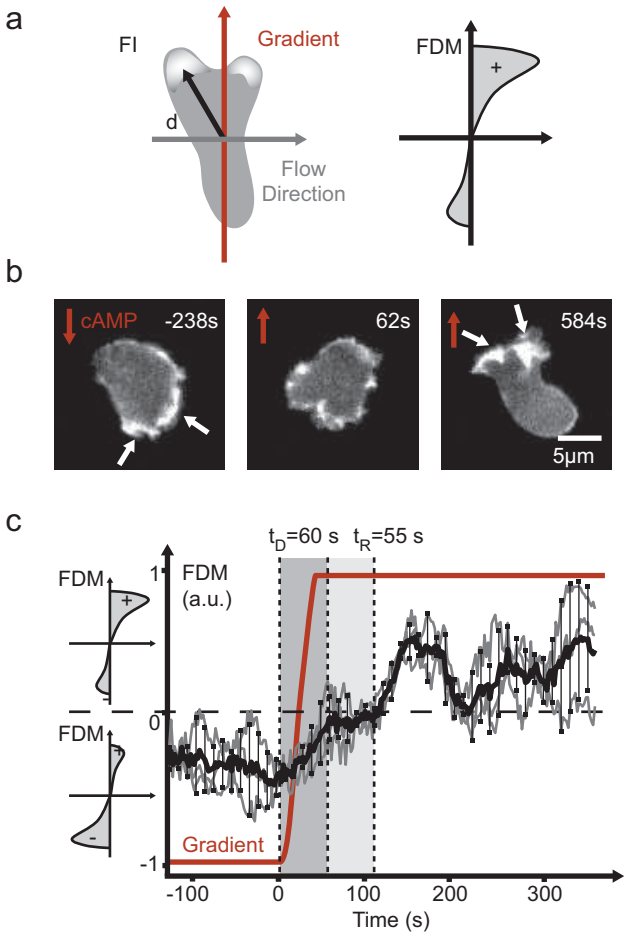

Figure 7.3: Quantitative analysis of the first migration type of re-polymerizing cells that constantly form fresh pseudopods to adapt to a switch in gradient direction. (a) A fluorescence distribution moment (FDM) is introduced to quantitatively describe the intracellular redistribution of actin polymerization dynamics. The FDM is defined as the integrated product of the fluorescence intensity FI of every pixel and its distance to the cell center of mass d. (b) An exemplary shown cell shows pronounced actin polymerization at its cell perimeter pointing upwards the chemotactic gradient (236 s). After the gradient is switched balanced actin polymerization is observed throughout the cell perimeter, (62 s), before the cell fully adapts to the new gradient and a pronounced polarization is observed again (584 s). (c) The amplitude of the FDM is plotted over 3 consecutive switches for one cell, yielding reproducible response behavior within tight error margins. We observe a response delay of $t_D = 60$ s and a reorganization time with undirected actin polymerization of $t_R = 55$ s. The exemplary shown cell adapts to the new gradient direction within 2 min [86].

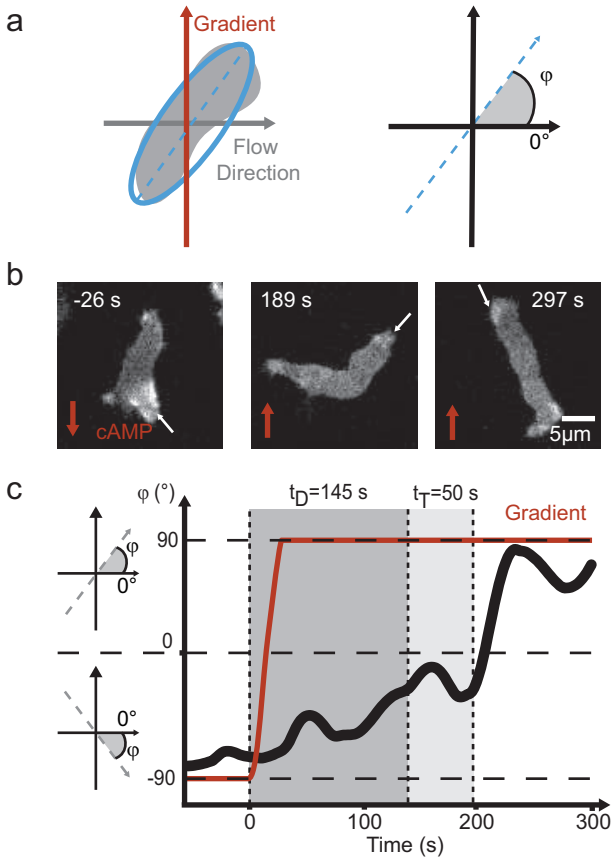

Figure 7.4: Quantitative analysis of the second migration type of stable polarized cells. (a) The migration angle is redefined as the angle φ between the orientation of the major axis of an ellipse fitted to the cell perimeter and the direction of the chemotactic gradient. (b) A stable polarized cell exhibits strong actin polymerization at its leading edge (white arrows). The cell is aligned with the recent stimulus (−26 s) before a switch in the direction of the chemotactic gradient occurs. After the gradient is switched the cells initiates an "U-turn" (189 s) to re-align with the new gradient direction (297 s). (c) The evolution of the migration angle yields a response delay of $t_D = 145\,\mathrm{s}$ before the cell starts to turn. After a turning time of $t_T = 50\,\mathrm{s}$ the cells again migrates upwards the chemotactic gradient [86].

(FDM). The FDM (Fig. 7.3a) is the integrated product of the Gfp intensity **FI** of each pixel and its displacement from the cell center of mass **d**,

$$\overrightarrow{FDM}| = | \sum_{PIXEL} FI \cdot \overrightarrow{d} |.$$

The FDM becomes positive if it points in the direction of the chemotactic gradient and negative if it is oriented in the opposite direction. A cell migrating in the direction of the chemotactic gradient exhibits a pronounced polymerization activity at the leading edge, which transfers into large FDM-values. For a more polarized, more elongated cell the FDM values further increase due to the increasing displacement of the leading edge to the cell center. As gradient switching in our experiment is defined in a definite axis, the amplitude of the FDM, $|\overrightarrow{FDM}|$, is sufficient to describe cell polarization within the alternating gradient fields.

FDM analysis facilitates quantitative description of the response behavior of re-polymerizing cells (Fig. 7.3b). The measurement is performed in a steep gradient of 35 pM/µm with an exposure time of $t_E = 600\,\mathrm{s}$ and a cell starved for 5.5 h. Cell response is plotted for 3 consecutive switches, resulting in a repeatable response within tight error margins (Fig. 7.3c). After the gradient is switched the exemplary cell keeps a polarization in the direction of the previous gradient for a delay time of $t_D = 60\,\mathrm{s}$. Afterward, we observe a re-organization time of balanced actin polymerization throughout the cell cortex , $t_R = 60\,\mathrm{s}$, resulting in small FDM values around 0. Overall, the cell aligns its polymerization activity with the recent chemotactic gradient after about 2 min.

Investigation of the dynamic intracellular re-distribution of actin polymerization activity by the FDM analysis, yields a quantitative description of the re-polymerization process of individual cells.

7.3 Stably Polarized Cells

The second migration type is defined by stably polarized cells that keep a constant leading edge in response to a change in gradient direction (Fig. 2.5, right). When the direction of the chemotactic gradient is altered, these cells step by step align with the new gradient direction. The cells perform

an "U-turn" (Fig. 7.1b). The constant leading edge results in a pronounced polarization of the cell, with actin polymerizing proteins accumulated at the cell front.

As the cells keep a stable polymerization front at the leading edge, FDM analysis will not give further insight into the adoption process of stably polarized cells. However, the elongated form of the polarized cells facilitate easy access to its alignment with the axis of the chemotactic gradient (Fig. 7.4a). The turning process is described by the orientation of the major axis of an ellipse fitted to the cell perimeter, in respect to the direction of the chemotactic gradient (Fig. 7.4c). Right after the gradient is switched, the exemplary cell still migrates in the direction of the previous stimulus before it starts to adjust to the new gradient direction (Fig. 7.4b) after a delay time of $t_D = 145\,\mathrm{s}$. When the turning process is initiated the cell gradually biases the migration into the direction of the new stimulus. Now, the cell is again aligned with the recent gradient after an additional turning time of $t_T = 50\,\mathrm{s}$. During the entire adaption process the cell will not form a de novo pseudopod but constantly keep its leading edge. Turning time and delay time yield a quantitative description of the turning process of the individual cells, like re-organization t_R and delay time t_D do for FDM analysis of re-polymerizing cells.

7.4 Shape Analysis

Analysis of the cell shape is performed using the ImageJ plugin CellEvaluator [98], developed by S. Youssef at the chair of J. O. Rädler, and the regionprops command of Matlab R2009b.

In this analysis we concentrate on cell shape, described by an ellipse fitted to the cell perimeter (Fig. 7.5a). Cell eccentricity is defined as the fraction of the distance of the ellipse foci and the length of the major axis. Eccentricity is therefore defined between 0 for a perfect circle and 1 for a straight line. The eccentricity of the ellipse is a measure for the elongation of the cells. A cell that exhibits a stable polarization, eventually elongates. In contrast, the steady re-polymerization of transiently polarized cell results in a rounder cell perimeter. Thus, cell eccentricity is used to distinguish between cells that exhibit a transient polarization in actin polymerization

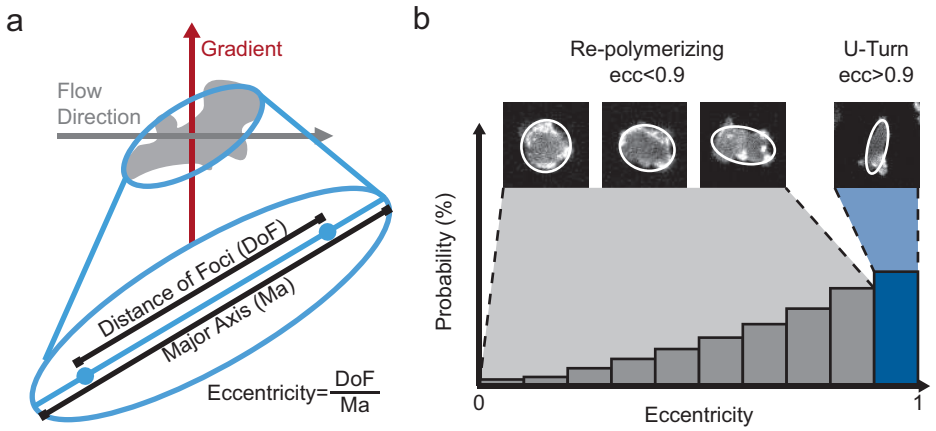

Figure 7.5: Shape analysis is based on the eccentricity of an ellipse fitted to the cell perimeter. (a) The regionprops function of Matlab is applied to fit an ellipse to the cell outlines. Eccentricity (ecc), the ratio of the distance of the ellipse foci to the length of the major axis, is used as a measure for cell elongation and therefore the polarization of the cell. The eccentricity is defined for values between 0 for a perfect cycle and 1 for infinite elongation. (b) The distribution of cell eccentricity is used to quantify the ratio of cells that perform the first (gray) or the second migration type (blue). The constant formation of fresh pseudopods in cells of the first migration type overall results in a rounder shape with cell eccentricities between 0-0.9, whereas stably polarized cells elongate with time, resulting in cell eccentricities above 0.9.

and cells that are stably polarized. We find the ratio of cells exhibiting cell eccentricities larger than 0.9 to yield a good estimate for the ratio of cells that perform an "U-turn" , whereas cells that re-polymerize in response to a switch in gradient direction exhibit eccentricity values smaller than 0.9 (Fig. 7.5b).

Chapter 8

Influence of Gradient Steepness on Cell Polarization

Shape analysis gives us the opportunity to quantitatively investigate the transition of re-polymerizing cells to stably polarized cell as it happens when the cells develop into the aggregation competent state (see section 2.2). Besides the ongoing starvation of the cells, gradient steepness has been described to influence the migratory chemotactic response [41].

In our experiments, we observe an increase in cell eccentricity (ecc), representing more stable polarized cells, with ongoing starvation. Furthermore, we identify a reduced influence of gradient steepness over time, pointing towards a decreased influence of the formation of fresh pseudopods on the migratory response with ongoing development of the cells.

Influence of gradient steepness is reduced with ongoing starvation of the cells

Cell shape analysis is performed for 3 independent measurements for shallow chemotactic gradients of $5-15\,{}^{\mathrm{pM}}/_{\mu\mathrm{m}}$ and for 4 independent measurements for steep chemotactic gradients from $20-80\,{}^{\mathrm{pM}}/_{\mu\mathrm{m}}$ for an exposure time of $t_E = 600\,\mathrm{s}$. More than 100 switching events are analyzed for each regime. Experiments are performed with cells at $5-7\,\mathrm{h}$ of starvation. In general, a starvation time of $6h$ is accepted as the onset of the transition into the aggregation mode in *D. discoideum* [33]. We distinguish between pre-aggregating cells that are starved for $5-6\,\mathrm{h}$ and aggregating cells starved for $6-7\,\mathrm{h}$.

In Fig. 8.1 individual pathways are plotted for a time span of 6 min after the switch in gradient direction is initiated. The cell tracks are color-coded with the mean eccentricity the cell is exhibiting during the 6 min period plotted, from $ecc < 0.5$ in blue to $ecc > 0.9$ in red. As a guide for the eye, the basic shape of the explored area, dismissing extreme cell paths, is highlighted in gray. The resulting ellipse is later used to qualitatively compare the directionality of the chemotactically induced migration in the two gradient regimes. The center of mass (com) of the sum of all cell pathways is indicated in the upper right corner of the individual plots, yielding a quantitative measure of the chemotactic bias of cell migration.

In pre-aggregating cells for a starvation time of $5-5.5$ h only short tracks are found for the steep gradient regime (Fig. 8.1a, left), and the shallow gradient regime (Fig. 8.1b, left). However, some cells already exhibit higher cell eccentricities and migrate over a much longer distance with a bias in the direction of the chemotactic gradient in the shallow gradient regime (red tracks in Fig. 8.1b, left). Comparison of the basic shapes of the areas explored by the cells in the steep (green) and the shallow gradient regime (blue) shows only slight differences but a modest bias of the migration direction is observed in the shallow gradient regime (Fig. 8.1c, left). At a starvation time of $5.5 - 6$ h, no clear change is found in the steep gradient regime (Fig. 8.1a, center left). In the shallow gradient regime, a significant ratio of the cells already exhibits large eccentricities and relatively long migration tracks (red tracks in Fig. 8.1b, center left). The cells in the shallow gradient regime show longer cell tracks and explore a larger area than in the steep gradient regime (Fig. 8.1c, center left). A chemotactic bias of cell migration is now observed in both regimes.

For aggregating cells, at $6 - 6.5$ h of starvation much longer cell paths then before are observed in the steep gradient regime, the cell clearly explore more area, with a pronounced bias in the direction of the chemotactic gradient (Fig. 8.1a, center right). In shallow gradients, many cells with large eccentricity values are found and a large area is explored by the cells. Even though there is a clear bias in the direction of the chemotactic gradient a wide spread distribution of cell displacement in all directions is observed (Fig. 8.1b, center right). The cells in the shallow gradient regime exhibit longer migration tracks than in steep chemotactic gradients, but the basic

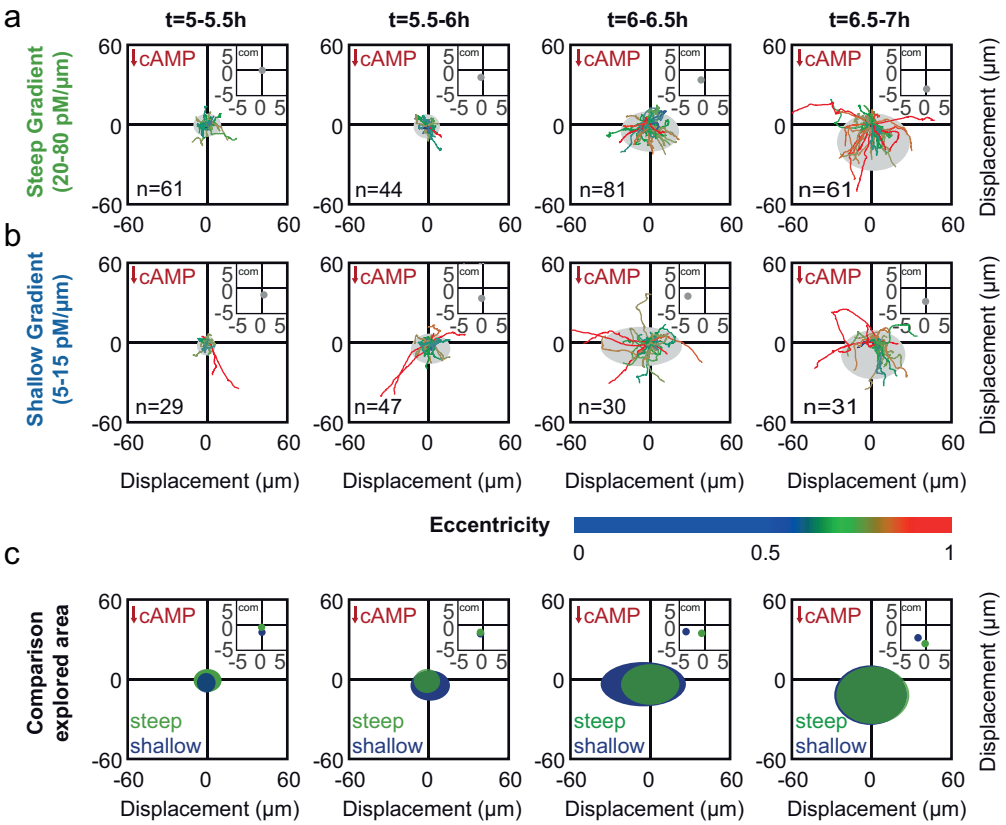

Figure 8.1: Individual cell trajectories for n cells over a time period of 6min after the gradient (red) is switched in the steep gradient regime between $20-80\,\mathrm{pM/\mu m}$ (green) and the shallow gradient regime between $5-15\,\mathrm{pM/\mu m}$ (blue). The mean ecc is color-coded with $ecc < 0.5$ in blue to $ecc > 0.9$ in red. The center of mass (com) of the sum of all individual tracks is indicated in the upper right corner. The area explored by the cells, dismissing extreme cell tracks is indicated in gray as a guide for the eye. (a) In the steep gradient regime only few extended cell tracks with low *ecc* are observed between $5-5.5\,\mathrm{h}$ and $5.5-6\,\mathrm{h}$. Longer tracks and a larger bias in cell migration is observed at $6-6.5\,\mathrm{h}$. At $6.5-7\,\mathrm{h}$ many cells with high ecc and a large bias in the direction of the chemotactic gradient is monitored. (b) In the shallow gradient regime, some highly elongated cells (red trajectories) are observed at $5-5.5\,\mathrm{h}$. At $5.5-6\,\mathrm{h}$ slightly more elongated cells are seen. At $6-6.5\,\mathrm{h}$ a much wider area is explored but only a small bias in the direction of the chemotactic gradient is monitored. At $6.5-7\,\mathrm{h}$ a clear bias in the direction of the chemotactic gradient and many cells with large ecc are observed. (c) Comparison of the explored area and the chemotactic bias in the steep (green) and the shallow (blue) gradient regime yields a larger explored area at $5.5-6\,\mathrm{h}$ and $6-6.5\,\mathrm{h}$ in the shallow gradient regime but not a larger chemotactic bias. At $6.5-7\,\mathrm{h}$ of starvation the explored area is almost identical but a slightly larger bias in the chemotactic migration is observed in the steep gradient regime.

shape of the explored area has its major axis perpendicular to the gradient direction (Fig. 8.1c, center right). Cells exhibit larger displacement perpendicular to the gradient direction than in the direction of chemotactic stimulation. However a clear bias in the direction of the gradient is still observed, whereas the perpendicular bias seems to be coincidental. At $6.5 - 7\,\mathrm{h}$ of starvation the cell tracks in the steep gradient regime become much longer, matching the pathways in shallow gradients. The long cell tracks are due to an increased eccentricity of the cells (red tracks in Fig. 8.1a, right). Yet, some of the cell migrate perpendicular to the chemotactic gradient. In the shallow gradient regime, it seems as cell migration is more biased and less cells migrate perpendicular to the chemotactic gradient than before (Fig. 8.1b, right). The explored areas seem to be less elliptical and the cells exhibit more bias in the direction of the chemotactic gradient direction (Fig. 8.1c, right). No significant difference between steep and shallow chemoattractant gradients is observed in the explored area. Yet, a larger chemotactic bias is observed in the steep gradient regime.

To sum up, we find an increase in the length of the cell tracks due to a higher eccentricity of the cells in both gradient regimes with ongoing starvation of the cells. Between $5 - 7\,\mathrm{h}$ of starvation the cells enter the aggregation phase and therefore establish a stable leading edge, resulting in more elongated cells. Yet, some differences are found. We observe cells with large eccentricities from the beginning of the experiment in the shallow gradient regime. In contrast, only few long migration tracks and cells with large eccentricities are observed in the steep gradient regime before $6.5\,\mathrm{h}$ of starvation. It seems as constant switching of the steep gradients prevents a stable polarization of the cells. Strikingly, at $6.5 - 7\,\mathrm{h}$ of starvation gradient steepness appears to not influence the migratory response anymore.

Decreased gradient steepness and ongoing starvation favor a stable polarization of the cells

Qualitative evaluation of individual cell trajectories provides first insight in the transition of single cells into aggregation competent cells. Yet, quantitative analysis of the cell eccentricity of entire cell ensembles promises additional insight into the control of the overall migration strategies by gradient steepness and ongoing starvation of the cells.

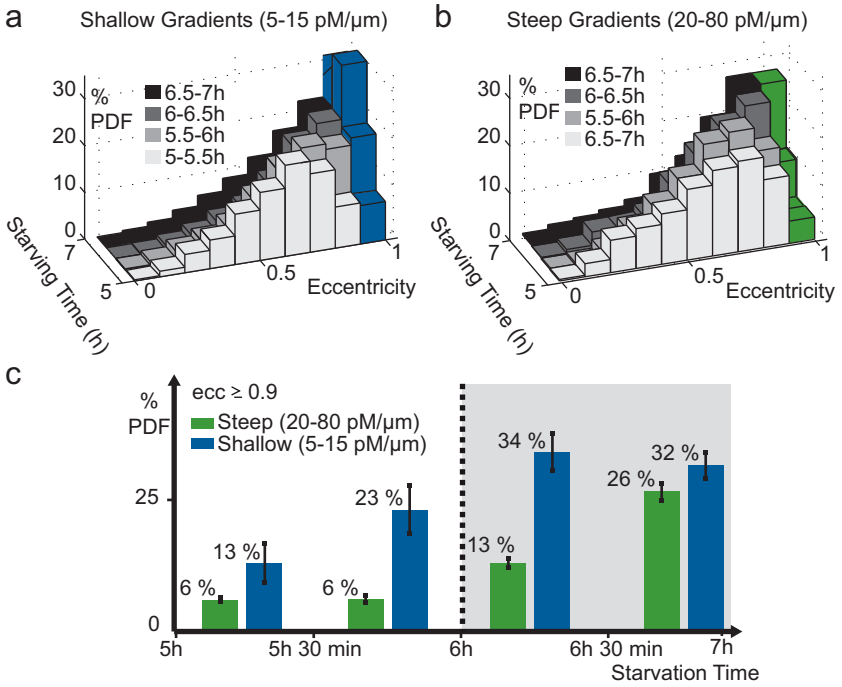

Figure 8.2: Cell eccentricity increases with ongoing starvation and decreasing steepness of the chemotactic gradient. (a) In the shallow gradient regime ($5-15\,\mathrm{pM/\mu m}$) more elongated cells are found from the start. The high eccentricity cells show a maximal ratio of 32% (blue). (b) In the steep gradient regime of chemoattractant gradients between $20-80\,\mathrm{pM/\mu m}$ a steady increase of cell eccentricity is found with ongoing starvation. Highly elongated cells mainly exhibit a cell eccentricity above 0.9 show a gradual increase from 6% to 26% (green). (c) Comparison of the ratio of cells exhibiting eccentricities larger than 0.9 yields 6% and 13% of highly elongated cells for the steep (green) and the shallow (blue) gradient regime at $5-5.5\,\mathrm{h}$ of starvation. For $5.5-6\,\mathrm{h}$ the ratio increases to 23% for in the shallow gradient regime while it remains constant for steep gradients (6%). For $6-6.5\,\mathrm{h}$ of starvation an increased percentage of 13% is found for steep gradient and 34% for shallow gradients. At the end of the measurement for $6.5-7\,\mathrm{h}$ of starvation, a large increase to 26% of highly elongated cells is found in the steep gradient regime, whereas about the same amount as before (32%) are found in the shallow gradient regime [86].

In both gradient regimes the mean cell eccentricity increases with ongoing starvation as the cell develop into aggregating cells (Fig. 8.2a, b). As already discussed in section 7.4, the ratio of cells exhibiting eccentricities larger than 0.9 yields a good estimate for the transition between repolymerizing cells and cells that keep a stable front (green and blue bars in Fig. 8.2a and b). At the start of the experiment at $5 - 5.5\,\mathrm{h}$ of starvation 6% of the cells in the steep gradient regime exhibit eccentricities above 0.9 (green bars in Fig. 8.2c) whereas more than double the cells exhibit a high elongation in shallow gradients (13%) (blue bars in Fig. 8.2c). For $5.5 - 6\,\mathrm{h}$ of starvation, the ratio of highly elongated cells further increases in the shallow gradient regime to 23% while in the steep gradient regime no change in the ratio of highly elongated cells is observed (6%).

In aggregating cells, at $6 - 6.5\,\mathrm{h}$ of starvation, the cells in the steep gradient regime start to get more elongated (13%) and in the shallow gradient regime the ratio of cells that exhibit an eccentricity larger 0.9 further increases to 34%. At the end of our measurements at $6.5 - 7\,\mathrm{h}$ of starvation a slight decrease in cell eccentricity within the error margin to 32% is found in the shallow gradient regime. However, cell elongation in the steep gradient regime largely increases (26%), almost matching the ratio observed in the shallow gradient regime.

The ratio of highly elongated cells increases in both gradient regimes over time. In accordance with the analysis of the individual cell tracks we find more highly elongated cells in the shallow gradient regime from the start. Interestingly, the ratio of highly polarized cells is not changing with ongoing starvation in the steep gradient regime before 6 h of starvation. After 6 h of starvation cells also start to elongated in the steep gradient regime, and the ratio of cells with eccentricities larger than 0.9 rises almost to the level of the shallow gradient regime. While the migratory behavior in steep chemotactic gradients differs from the migration in shallow gradients in pre-aggregating cells, this effect seems to vanish with ongoing starvation.

The influence of chemotactic gradient steepness on cell migration decreases with ongoing cell development

Cell shape analysis and investigation of individual cell trajectories both show a drastic change in the migratory behavior of chemotactic cells to-

wards stably polarized cells with ongoing transition into aggregation competent cells. Previous publications state that a difference in the formation of pseudopods in response to a change in the direction of the chemotactic gradient depends on gradient steepness [41]. Our findings agree with these reports as long as the cells are starved for less than 6.5 h. Here, we find a higher ratio of cells with an eccentricity larger than 0.9 and longer cell trajectories, pointing towards more stable polarized cells in the shallow gradient regime. However, in contrast to the migratory behavior before 6.5 h of starvation, cell response between $6.5 - 7$ h of starvation is less depending on the shape of the chemotactic gradient. The individual cell tracks in the steep and the shallow gradient regime look very similar (Fig. 8.1) and the ratio of highly elongated cells converges (Fig. 8.2). We conclude that the migratory response shifts towards the second type of stably polarized cells with ongoing starvation, independently of the steepness of the chemotactic gradient. Our findings point towards a decreased influence of PI3-Kinase based formation of fresh pseudopods on chemotactic migration with ongoing starvation of the cells.

Chapter 9

Starvation Time Dependent Influence of PI3-Kinase

Formation of fresh pseudopods depends on the formation of a PIP2/PIP3 gradient by PI3-Kinase based phosphorylation of PIP2 at the leading edge, which enables the cells to bias actin polymerization in the direction of the chemotactic stimulation.

Experiments performed with the drug LY294002 (LY) inhibiting multiple PI3-Kinases, perturb the phosphorylation of PIP3 in response to chemotactic stimulation [75]. Consequentially, the formation of fresh pseudopods in the direction of the chemotactic gradient is reduced. Here, we find the previously made assumption that the influence of PI3-Kinase on chemotactic migration vanishes with ongoing development of the cells, validated. We also observe a negative effect of PI3-Kinase on the chemotactic efficiency for cells starved for more than 6.5 h.

PI3-Kinase perturbation leads to an enhanced confinement to the axis of gradient switching in aggregating cells

Individual cell tracks for more than 150 switching events for cells perturbed in PI3-Kinase over a starvation period between $5-7\,\mathrm{h}$ in the steep gradient regime ($20-80\,{}^{\mathrm{pM}}/_{\mu\mathrm{m}}$) are compared to the cell trajectories of untreated cells in the same gradient regime (also see Fig. 8.1a), to investigate the starvation time dependent influence of PI3-Kinase on the chemotactic response. At the start of the experiment at $5-5.5\,\mathrm{h}$ of starvation, LY-treated cells that

are deficient in PI3-Kinase exhibit shorter individual trajectories as the untreated Lim-wildtype cells (Fig. 9.1a, b, left). The explored area is therefore quite small (orange) and no chemotactic bias is found for both cell types (Fig. 9.1c, left). At $5.5 - 6\,\mathrm{h}$ the cells deficient in PI3-Kinase, explore a larger area as at the start of the experiment. The main portion of the cells shows similar tracks than for untreated cells. However, long migration tracks with relatively large cell eccentricities are observed for LY-treated cells (green in Fig. 9.1a, b, center left). Yet, the main area explored, when extreme cell trajectories are dismissed, and the chemotactic bias by the cells perturbed in PI3-Kinase and the Lim-wildtype cells are almost identical (Fig. 9.1c, left).

For aggregating cells at $6 - 6.5\,\mathrm{h}$ of starvation, we still see similar migration trajectories for cells deficient in PI3-Kinase and Lim wildtype cells (Fig. 9.1a, b, center right). Only a few cells that exhibit long trajectories are found for LY-treated cells. Still, it seems that the trajectories of the cells deficient in PI3-Kinase are more confined to the axis of gradient switching, as can be seen by the explored areas (Fig. 9.1c, center right). Consequentially, a slightly larger chemotactic bias is observed for LY-treated cells. Further increase in cell eccentricity is observed for both cell types at $6.5 - 7\,\mathrm{h}$ of starvation. Migration trajectories look much the same but almost all cells that are treated with LY, persitently migrate towards the chemotactic stimulus (Fig. 9.1a, b, right). In contrast, we find some cells that migrate perpendicular to the gradient direction for untreated cells, resulting in a more spread out area that is explored. The area explored by the LY-treated cells is much more confined into the axis of gradient switching and a larger chemotactic bias is again found for cell deficient in PI3-Kinase (Fig. 9.1c, right).

Suppression of the PIP3 phosphorylation surprisingly seems to increase the directionality of chemotactic migration and therefore the bias of the combined center of mass of the cell tracks. For pre-aggregating cells, analysis of the individual cell tracks shows only slightly more extended trajectories for cells deficient in PI3-Kinase, whereas significant enhancement of the persistence in the direction of the chemotactic gradient is observed for aggregating cells. We find evidance that suggest that PI3-Kinase inhibition increases the directionality of chemotactic migration at long starvation times.

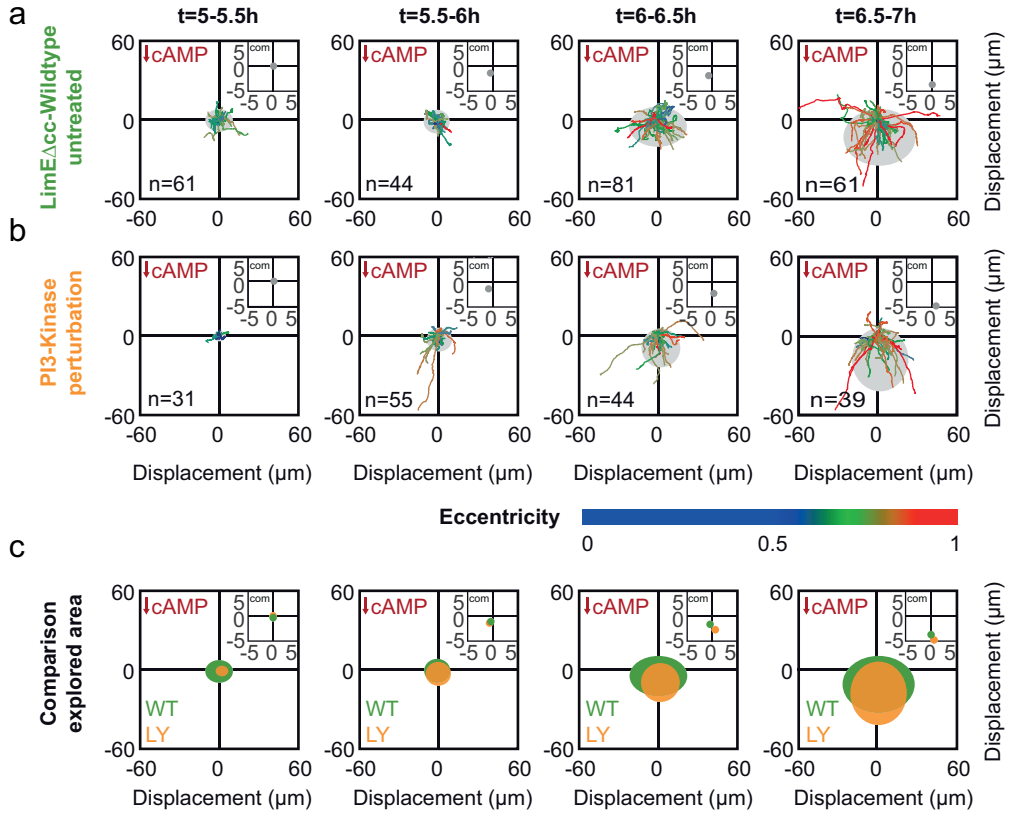

Figure 9.1: Individual cell trajectories for n cells for a time period of 6min after the gradient (red) is switched for Lim-wildtype (WT) cells and cells treated with the PI3-Kinase inhibitor LY 294002 (LY) in the steep gradient regime between $20 - 80\,\mathrm{pM/\mu m}$. The mean ecc is color-coded with $ecc < 0.5$ in blue to $ecc > 0.9$ in red. The center of mass (com) for the sum of all cell trajectories is indicated at the upper right corner.The area explored by the cells, dismissing extreme cell tracks is indicated in gray as a guide for the eye. (a) At $5 - 5.5\,\mathrm{h}$ of starvation hardly any migration is observed for Lim-wildtype cells. At $5.5 - 6\,\mathrm{h}$ a slight bias in the direction of the chemotactic gradient is found. At $6 - 6.5\,\mathrm{h}$ of starvation the cell trajectories extend and some cells with large ecc (red tracks) are observed. The trajectories experience a pronounced chemotactic bias. At $6.5 - 7\,\mathrm{h}$ many cells with large ecc and long tracks and the largest chemotactic bias are observed. (b) For $5 - 5.5\,\mathrm{h}$ almost no migration is fund for LY-treated cells. At $5.5 - 6\,\mathrm{h}$ still mostly short cell trajectories are observed but a few elongated cells experience extended trajectories. At $6 - 6.5\,\mathrm{h}$ a larger area is explored yielding more cells with large ecc. At $6.5 - 7\,\mathrm{h}$ many cells experience large ecc and a large chemotactic bias is observed. (c) At $5 - 5.5\,\mathrm{h}$ no chemotactic bias is found for both cell types but the LY-treated cells (orange) explore a smaller area than the Lim-wildtype cells (green). At $5.5 - 6\,\mathrm{h}$ the explored area are almost identical but the cells deficient in PI3-Kinase experience a larger chemotactic bias. At $6 - 6.5\,\mathrm{h}$, the explored area is more confined for the LY-treated cells. At $6.5 - 7\,\mathrm{h}$ the confinement of the cells deficient in PI3-Kinase to the axis of gradient switching becomes even more obvious, resulting in a larger chemotactic bias.

PI3-Kinase inhibition increases cell eccentricity in pre-aggregating cells

In contrast to the individual cell tracks discussed above, we observe a significant increase in the ratio of highly polarized cells (green and orange bars in Fig. 9.2 a, b) from the start of the experiment. At $5-5.5\,\mathrm{h}$ of starvation the ratio of cell with eccentricities larger than 0.9 increases form 6% to 18% if PI3-Kinase is perturbed. Almost the same result is found for $5.5-6\,\mathrm{h}$ of starvation (6% and 17%). For aggregating cells at $6-6.5\,\mathrm{h}$ of starvation, the ratio of highly elongated cell increase in LY-treated cells as it had already been described for untreated cells (also see Fig. 8.2a). However, only a slight increase is observed for cells deficient in PI3-Kinase (20%), whereas the number of cells with an eccentricity larger than 0.9 more than doubles in Lim-wildtype cells (13%). Similar to the influence of gradient steepness, the influence of PI3-Kinase perturbation on cell eccentricity is also diminished for a starvation time of $6.5-7\,\mathrm{h}$. Here the ratio of highly elongated cells in untreated cells (26%) almost matches that of cells perturbed in PI3-Kinase (30%).

The higher elongation of cells perturbed in PI3-Kinase points towards a shift to stably polarized cells right from the start of the experiment. However starting at 6 h of starvation the influence of PI3-Kinase is strongly diminished, pointing towards an decreased influence of PI3-Kinase on the migratory response for aggregating cells. Comparable to the decreased influence of gradient steepness with ongoing starvation of the cells, perturbation of PI3-Kinase also seems to be diminished at long starvation times.

PI3-Kinase promotes re-polymerization in pre-aggregating cells

The formation of new pseudopods based on PI3-Kinase results in a reorganization of the cell cortex and therefore a transient accumulation of actin polymerization at the cell side facing the recent stimulus [49]. Perturbing PI3-Kinase is expected to hinder the cell to adjust to a switch in gradient direction by the formation of fresh pseudopods.

Analysis of the fluorescence distribution moment (FDM) shows a significant difference for perturbed and unperturbed cells in the re-polymerization dynamics in response to a switch in gradient direction. FDM analysis is per-

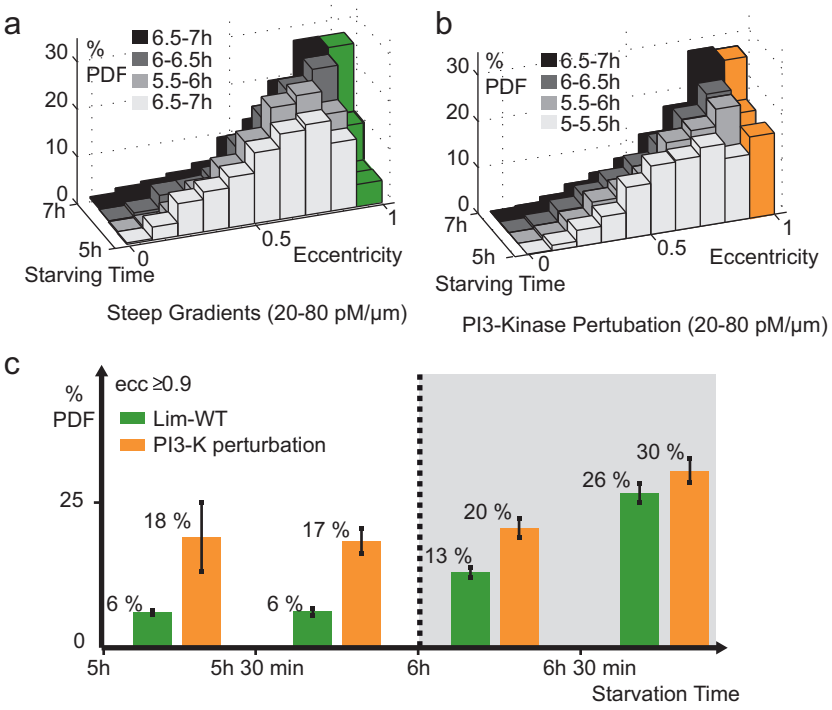

Figure 9.2: Cell eccentricity is increased by PI3-Kinase perturbation through LY 294002 (a) Evolution of gradient steepness in steep gradient regimes for untreated cells (also see Fig. 8.2a). (b) The overall distribution of untreated and cells with PI3-Kinase perturbed, seems to be relatively unchanged. However, the ratio of cell exhibiting cell eccentricities above 0.9 is clearly increased (orange). (c) For a starvation time of $5 - 5.5\,\mathrm{h}$ much more elongated cells (18%) are found for PI3-Kinase perturbation than in untreated cells (6%). For $5.5 - 6\,\mathrm{h}$ both values stay almost constant (6% and 17%). After $6 - 6.5\,\mathrm{h}$ of starvation, the value of highly elongated cells largely increases for untreated cells (13%) and slightly increases for PI3-Kinase perturbed cells (20%). At the end of the measurements at $6.5 - 7\,\mathrm{h}$ the untreated cells almost yield the same amount of elongated cells (26%) as for cells perturbed in PI3-Kinase (30%) [86].

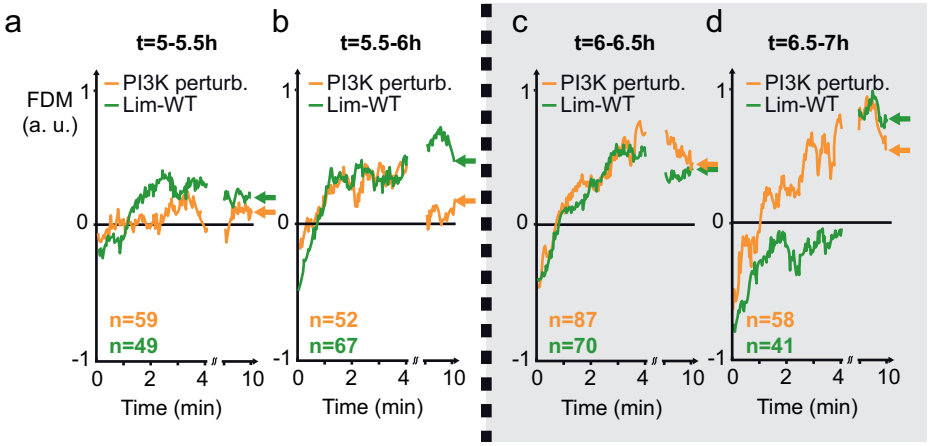

Figure 9.3: Influence of PI3-Kinase on the re-polymerization behavior of n chemotactic cells quantified by the FDM analysis. All cells with an $ecc < 0.9$ that did not touch or leave the observation area during the switching period are plotted. (a) For pre-aggregating cells at $5 - 5.5\,\mathrm{h}$ of starvation, the re-polymerization in response to a switch in gradient direction is only slightly pronounced in both cell types but Lim-wildtype cells (green) keep their remote polarization throughout the switching period. (b) At $5.5 - 6\,\mathrm{h}$ PI3-K perturbation (orange) largely reduces the cells ability to built a polymerization front in the direction of the chemotactic gradient as it is observed for untreated cells. (c) For aggregating cells at $6 - 6.5\,\mathrm{h}$ no effect of PI3-Kinase perturbation is observed, both cell types exhibit the same polarization at the end of a switching period. (d) PI3-Kinase perturbation is promoting a fast re-polymerization of the cells, whereas untreated cells are only slowly adjusting their cell polarization to the recent gradient direction at $6.5 - 7\,\mathrm{h}$ of starvation[86].

formed for 236 and 227 switching events with Lim-wildtype cells and cells perturbed in PI3-Kinase, respectively. For pre-aggregating cells, PI3-Kinase perturbation (orange) reduces the cell's ability to establish a polarization in the direction of the chemotactic gradient. Between $5-5.5$ h of starvation there is only a slight effect visible (Fig. 9.3a), but for $5.5-6$ h untreated cells (green) experience a pronounced re-polymerization behavior, whereas PI3-Kinase perturbed cells are not capable to keep up their polarization (Fig 9.3b).

For aggregating cells, the influence of PI3-Kinase perturbation again changes drastically (Fig. 9.3c, d). At $6-6.5$ h of starvation, LY-treated and Lim-wildtype cells, show similar re-polymerization characteristics, yielding a comparable amplitude of the FDM after 10 min. Surprisingly, at $6.5-7$ h of starvation, cells deficient in PI3-Kinase show faster re-polymerization when compared to untreated cells. Even though, both cell types yield comparable FDM values at the end of the switching period, it is obvious that perturbation of PI3-Kinase hinders fast adjustment of the cells to changing gradient direction in our experimental design for long starvation times.

To sum up, we find a drastic change in the influence of PI3-Kinase perturbation at 6 h of starvation as it has also been observed for cell shape analysis and individual cell trajectories. At the start of the experiment PI3-Kinase seems to promote actin polymerization dynamics and therefore induced the first migration type of re-polymerizing cells as it had to be expected. Yet, after 6 h of starvation the effect of PI3-Kinase perturbation first diminishes, and later on rapid adjustment to the recent gradient direction seems to be even favored by perturbation of PI3-Kinase.

PI3-Kinase is less constitutive in aggregating cells

In conclusion, we find a switch in the influence of PI3-Kinase on the migratory behavior of chemotactic cells at 6 h of starvation. However on a first sight, analysis of individual cell trajectories, the distribution of cell eccentricity and the fluorescence distribution moment (FDM), show different results.

PI3-Kinase is known to accumulate at the tip of freshly formed pseudopods in response to chemotactic stimulation [49]. For the gradient switching experiments described in this thesis, effective chemotaxis based on PIP3

phosphorylation would result in re-polymerization and the formation of new pseudopods at the former rear of the cell. This migration behavior results in less elongated cells only exhibiting a transient polarization that is intracellularly switched according to the chemotactic gradient.

In pre-aggregating cells, no significant difference in LY-treated and Lim-wildtype cells is observed for a qualitative analysis of the cell trajectories. Only few cells that experience extended migration tracks and large mean eccentricities are found for PI3-Kinase perturbation for starvation times of $5-6\,\mathrm{h}$. Yet, distribution of cell eccentricities and FDM analysis yield an influence of PI3-Kinase perturbation in pre-aggregating cells. The ratio of cells with eccentricities larger than 0.9 in cells deficient in PI3-Kinase exceeds the ratio of untreated cells by a factor of three.

The difference between the analysis of single trajectories and the distribution of cell eccentricity might be due to an underestimation of the trajectories of highly elongated cells. Single cell tracks are only analyzed if the cell is tracked over the entire switching period. As elongated cells in general migrate relatively fast, they are more likely to touch other cells or leave the observation area. Therefore trajectories of elongated cell might be dismissed.

For aggregating cells, that are starved for $6-6.5\,\mathrm{h}$, we find a diminished influence of PI3-Kinase perturbation on cell eccentricity, as it was expected. Astonishingly, cell trajectories point towards a more effective directed migration for cells deficient in PI3-Kinase when compared to untreated cells. The superior confinement in the axis of gradient switching for individual cell tracks is supported by FDM analysis that yield a faster adjustment to the altered gradient direction for LY-treated cells at $6.5-7\,\mathrm{h}$ of starvation.

Bosgraf et al. propose enhanced persistent migration for cells deficient in PI3-Kinase which seems to also lead to an enhanced persistence in our setup. However, in micropipette assays wildtype cells outperform cells with suppressed PI3-Kinase activity [71]. In contrast, we find an advantage of cells perturbed in PI3-Kinase at long starvation times for our experimental assay. One possible explanation is that the formation of new pseudopods causes the cell to deviate from gradient direction, as well as it helps to reorient lost cells. For the cells in our setup that are already aligned with the axis of the chemotactic gradient, the loss of PI3-Kinase results in an

enhanced directionality of the cell.

To sum up, we find PI3-Kinase to promote re-polymerization in pre-aggregating cells and with ongoing development of the cells a diminished influence of PI3-Kinase on chemotactic efficiency is observed.

Chapter 10

Conclusion & Outlook: Probing the Intracellular Regulatory Network

In my thesis, I developed a Chemotactic Gradient Generator and established its potential for the investigation of the effect of gradient steepness, ongoing cell starvation and perturbation of distinct signaling pathways on the eukaryotic chemotactic response. Homogeneous chemotactic gradients that directly evolve within the flow chamber by diffusion at the stream interfaces extend over several hundred microns, enabling studies of large samples of cells and therefore a quantitative description of chemotactic migration. The three inlet design of the double T-junction chamber enables rapid modification of the individual streams, resulting in controlled exposure of the cells to alternating gradient direction.

10.1 Chemotactic Migration in Alternating Gradients

Gradient switching at the time scales of the regulatory network

Besides a broad statistical analysis, rapid perturbations of the intracellular regulatory network are necessary to gradually disentangle the complex interplay of multiple parallel pathways in intracellular signaling [81]. Gradient switching has to be fast enough to probe the single steps of chemotaxis

at their intrinsic time scales.

Previous reports observed a first peak of F-actin polymerization approximately 10 s after the chemotactic stimulus is applied [20, 54, 55]. This first step referred to as directional sensing is followed by a less pronounced but steadier second peak of F-actin polymerization after 1 min.

For the Chemotactic Gradient Generator (CGG), finite element calculations (FECs) yield a theoretical limit for gradient switching of $t_E = 1.5\,\mathrm{s}$, well within the reported timescales of the chemotactic response (see Fig. 5.6). In live cell experiments, gradual increase of the switching frequency to 0.1 Hz, yields a "chemotactically trapped" cell state (see Fig. 6.2). Accurate control of the gradient direction at high switching frequency enables us to separate the individual feedback motifs of directional sensing and migration in response to homogeneous chemotactic gradients. Previously, investigation of directional sensing had only be achieved in response to uniform pulses of chemoattractant [55] or by pharmaceutical inhibition of the migratory apparatus of the cell [8, 58]. We, for the first time, address directional sensing in response to rapidly alternating homogeneous gradients in wildtype cells. Chemotactic cell trapping in the CGG, establishes the capability of our setup to address the chemotactic response of *D. discoideum* at its intrinsic time scales (see chapter 6).

Starvation time dependent effect of gradient steepness

At long exposure times, cell response to a change in the direction of the chemotactic gradient is determined by two types of chemotactic migration that differ in their mechanism of pseudopod formation [41, 76]. The first migration type forms fresh pseudopods in the direction of the altered chemotactic gradient [39], whereas the second gradually adjusts its migration direction by splitting of the leading edge [38].

Ongoing development of the cells during starvation determines whether they favor the first or the second type of migration. With the transition into aggregating cells, the cells polarize and are more likely to keep a steady leading edge. Still, gradient steepness has also been described to influence the migratory response [41]. Previous reports found that PI3-Kinase is more important in steep gradients than in the shallow gradient regime [71, 106]. Accumulation of PI3-Kinase at the membrane in response to chemotactic

stimulation leads to the formation of a pseudopod pointing in the direction of the chemotactic gradient, as it is suggested to occur in cells performing the first migration type.

Controlled gradient switching in our experimental assay facilitates a quantitative analysis of which migratory response is favored dependent on gradient steepness and ongoing cell development. To experimentally characterize the response behavior of both migration types, we introduced a fluorescence distribution moment (FDM) and the migration angle φ. FDM analysis readily describes the re-polymerization behavior of the first migration type (see Fig. 7.3), whereas the orientation of the cell with respect to gradient direction illustrates the response behavior of cells that perform a "U-Turn" (see Fig. 7.4).

We performed measurements in steep chemotactic gradients of $20 - 80\,{}^{\mathrm{pM}}/_{\mu\mathrm{m}}$ and more shallow gradients of $5 - 15\,{}^{\mathrm{pM}}/_{\mu\mathrm{m}}$ for cells that are starved for $5 - 7\,\mathrm{h}$ (see chapter 8). At the start of the measurements, we find more stably polarized cells in the shallow gradient regime as has been predicted [41, 106]. However, the ratio of highly elongated cells in the steep gradient regime quickly rises after 6 h of starvation. At 7 h of starvation, the number of stably polarized cells in the steep gradient regime almost matches the number in the shallow gradient regime (see Fig. 8.2).

To summarize, large sample numbers and controlled switching of the gradient direction in the CGG facilitates a quantitative analysis of chemotactic migration. We find the effect of gradient steepness strongly reduced after 6 h of starvation, pointing towards a diminished significance of PI3-Kinase based formation of fresh pseudopods that had been qualitatively described in previous reports [41].

Starvation time dependent influence of PI3-Kinase

Recently, several reports point out that multiple pathways which simultaneously mediate the chemotactic response in eukaryotic cells are necessary for effective directed migration [5, 40, 103, 107]. However, how the individual pathways interact depending on the initial conditions of the chemotactic stimulation is up to now not understood.

One of the multiple pathways that is suggested to steer the cell is the formation of fresh pseudopods by PI3-Kinase. In pre-aggregating cells, mea-

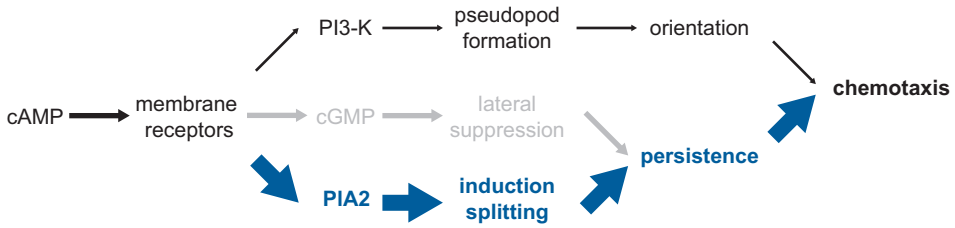

Figure 10.1: Our results suggest that with ongoing starvation ($> 6\,\mathrm{h}$) PI3-Kinase based formation of fresh pseudopods becomes less important for effective chemotactic cell migration. PlA2 induced splitting of the leading edge might instead be more important resulting in more highly elongated cells (blue).

surements with the PI3-Kinase inhibitor LY 294002 confirm the importance of PI3-Kinase for the re-polymerization process of the cells at $5-6\,\mathrm{h}$ of starvation (see chapter 9). Here, cells inhibited in PI3-Kinase are more likely to be elongated (see Fig. 9.2) and show less efficient re-polymerization after the gradient is switched (see Fig. 9.3a, b).

However, after $6\,\mathrm{h}$ of starvation the dependence of the cell response on PI3-Kinase changes drastically. At first, it seems that the influence of PI3-Kinase vanishes as almost no effect from its inhibition is found in the FDM analysis. Yet, after $6.5\,\mathrm{h}$ of starvation, PI3-Kinase inhibition seems to astonishingly favor a fast re-polymerization behavior (see Fig. 9.3d) and we find a superior bias of the individual cell trajectories in the direction of gradient switching as compared to wildtype cells (see Fig. 9.1).

The dependency of PI3-Kinase mediated formation of fresh pseudopods on the starvation time of the cells has not been described before, however it has been shown in micropipette assays that wildtype cells outperform cells that are deficient in PI3-Kinase [71]. Yet, for the controlled gradient switching that is used in our experiments a quantitative analysis of the effect of PI3-Kinase inhibition on the chemotactic response becomes possible and it seems as if cells deficient in PI3-Kinase show a more effective chemotactic response than wildtype cells after $6.5\,\mathrm{h}$ of starvation.

In conclusion, we find strong evidence that with ongoing development of the cells during starvation, the migratory response becomes less dependent on PI3-Kinase mediated formation of fresh pseudopods and stably polarized cells determine chemotactic migration. Our results suggest that the balance between the two key chemotactic pathways of PI3-Kinase based formation of new pseudopods and Phospholipase A2 mediated pseudopod splitting shifts

towards the latter with ongoing starvation (Fig. 10.1). Consequently, the chemotactic compass [56], mediated by PI3-Kinase, seems to be important for pre-aggregating cells, while the migration of aggregating cells is better described by the pseudopod-centered view [76].

One possible explanation for this starvation time dependence could be that a rapid change in migration direction is important for *D. discoideum* during early starvation when new aggregation centers are still forming, whereas it is more important for aggregating cells to persistently migrate towards the already established aggregation centers.

10.2 Beyond PI3-Kinase and *Dictyostelium discoideum*

Increasing the switching frequency

Chemotactic cell trapping resulted in stalled migration at an exposure time of $t_E = 10\,\mathrm{s}$. One of the remaining questions is whether the cells are still able to resolve the gradient switching for even faster exposure times. In order to reliably switch close to the theoretical limit of exposure time at $t_E = 1.5\,\mathrm{s}$, residual effects such as the response characteristics of the pressure pumps or the intrinsic noise of the stepper motor of the syringe pump need to be reduced.

The group of Prof. Whitesides introduced microfluidic valves for PDMS flow chambers [108]. Here, the flow chamber itself is on top of another PDMS duct that is inflated with gas (Fig. 10.2). A fast rise in the applied pressure at the valve becomes available due to the large reservoir of a gas bottle. Spreading of the valve results in a decreasing radius of the flow channel and therefore a reduced flow rate. The reservoirs could than be kept at a constant pressure, thus eliminating noise originated from the pumps and the inflow velocity would be controlled at a high accuracy by the radius of the flow channel at the position of the valve.

Starvation time dependent influence of parallel pathways

The broad statistical analysis that is facilitated by the large spatial extension of the gradient fields produced in our flow chamber allows for the

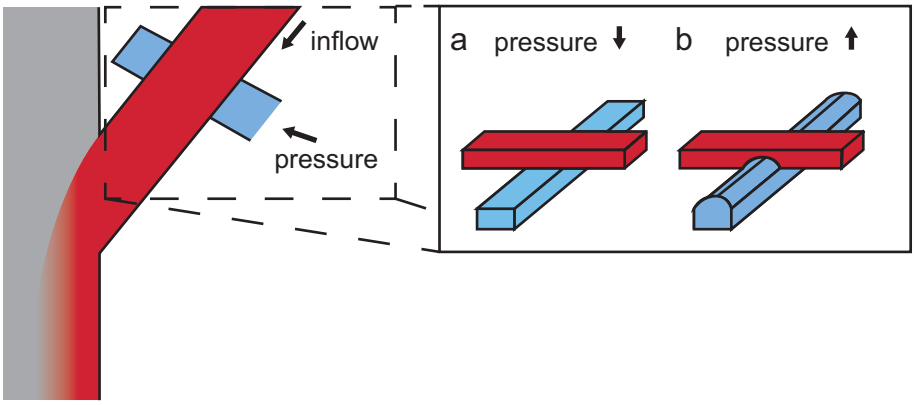

Figure 10.2: PDMS flow valves instead of micrometer valves used in the current setup could facilitate faster transition between opposing gradient fields. The PDMS valves base on a second duct perpendicular to the flow that is inflated by pressure (blue). (a) Low pressure application opens the flow channel and facilitates high flow velocities. (b) Increasing the pressure application allows for precise adjustment of the flow resistance.

investigation of the effect of single chemotactic pathways on directed migration. We demonstrated that the influence of PI3-Kinase on the migratory response is vanishing with ongoing development of the cells. Our results suggest an increased influence of PlA2 mediated splitting of the leading edge at large starvation times. Therefore, inhibition of PlA2 by p-bromophenacyl bromide [75] would be a consistent next step.

Additional experiments should also include the role of the uropod and its function in cell polarization. A prime candidate is the motor protein Myosin II which is involved in the contraction of the rear of the cell and therefore has a large influence on lateral pseudopod suppression.

Migration control in alternating gradient fields

Stimulation with chemoattractant gradients makes our experimental design an obvious choice for the investigation of the chemotactic response. Yet, the controlled initiation of changes in the migration direction of the cell makes our flow chamber also an ideally suited setup to explore migration in general.

Recently, much interest has been generated by the question of what role blebbing plays in cell migration. Spontaneous formation of cell protrusions by a detachment of the cell membrane from the cytoskeleton is referred to

as a bleb. At the first glance, blebs seem to be uncontrolled ruptures of the cytoskeleton, however recent studies suggest a large influence of blebbing on eukaryotic migration. Cells that migrate within a tense tissue particularly seem to functionalize bleebing in order to protrude [109]. Bleebing is also observed in *D. discoideum* [110] and is likely used to direct migration in the direction of the chemotactic gradient [72]. However, it is still not know precisely how blebbing is used to direct cell migration. Forcing the cells to repeatedly change their direction of migration in a controlled manner yields the necessary statistical footwork to further investigate how they depend on the controlled formation of pseudopods and the directed blebbing of the cell membrane.

Chemotactic response of mammalian cells

As already mentioned, blebbing is a defining feature of cells which migrate through tissue which applies in particular to mammalian cells. Preliminary measurements with endothelial HUVEC cells performed in our flow chamber, show that the CGG can easily be adapted to investigate these cells (Fig. 10.3). Due to the smaller diffusion coefficients of growth factor proteins when compared to the diffusion coefficient of cAMP, modification of the experimental settings becomes necessary.

Reduction of the inflow velocities facilitates the generation of homogeneous growth factor gradients and their controlled application to the cells. It has to be noted that slower flow velocities will also result in a larger transition time for a switch in the direction of the chemotactic gradient. Yet, most mammalian cells migrate at much lower speed than *D. discoideum* and much smaller switching frequencies need to be applied.

Furthermore, the large extension of the gradients produced in the CGG allow for the exposure of whole cell ensembles and therefore holds the potential to be extended to entire cell tissues. In embryogenesis and angiogenesis, entire cell tissues are directed by concentration gradients. This makes our experimental design a promising prospect for the investigation of coordinated chemotactic cell migration.

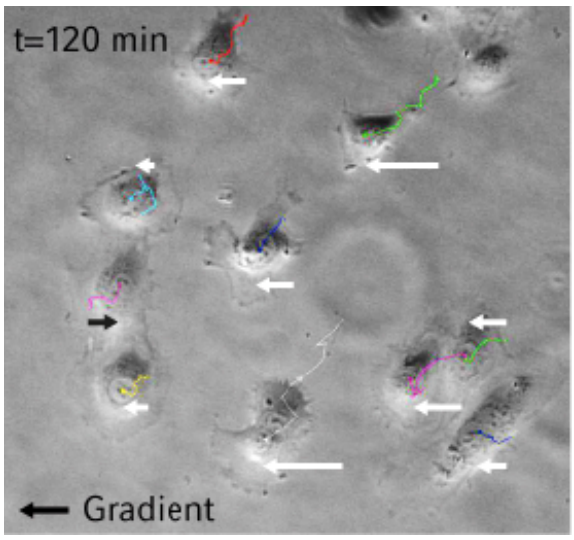

Figure 10.3: Endothelial cells migrate in a gradient of fetal calf serum. A biased motion is observed for the stimulated cells over 120 min of exposure (white arrows).

Appendix A

Material & Methods

Microfluidic function generator

In our setup, we use 'µ-slide 3in1' microfluidic chambers (Ibidi, Munich, Germany) with three$0.4x1.0\,\mathrm{mm}^2$ inflows that converge under an angle of $\alpha = 32°$to the main channel of dimensions $0.4x3.0x23.7\,\mathrm{mm}^3$ (Fig. 5.2). Both side flows (SF) are connected to reservoirs, built from two 20 ml syringes (Braun Melsungen AG, Melsungen, Germany), separately connected to a customized 'Suction Control' pressure pump (Nanion, Munich, Germany). Two micrometer valves (Upchurch Scientific, Oak Harbor, WA, USA) reduce the flow velocities at the SFs and allow for precise adjustment of the inflow velocities applied to the side inflows. The central flow (CF) is connected to an 'Infusion' syringe pump (TSE Systems, Bad Homburg, Germany), which generates a stable flow of 1 ml/h. Measurements are performed with an Axiovert 135 TV microscope (Zeiss, Oberkochen, Germany), with LD Plan-Neofluar objectives of 20 x / 0.50 N.A. and 40 x / 0.75 N.A. magnification (Zeiss, Oberkochen, Germany) in combination with a DV2 DualView system (Photometrics, Tucson, AZ, USA). The dual view system allows for simultaneous observation of cells with a Lim-Gfp label and the fluorescent dye Alexa 568, used to mimic the concentration distribution of cAMP (also see Fig. 5.3).

Cell culture

All cells are derived from the *D. discoideum* AX2 strain. Cells with Free-Gfp expressed in AX2 background [111], are used for cell tracking, while cells

with LimEΔcc-Gfp expressed in a LimEΔcc-null AX2 background [112] are used for FDM analysis. LimEΔcc mutant cells are grown in AX2 nutrition medium, containing 10 µg/ml Geneticin 418 disulfate salt (G418) (Sigma-Aldrich, St. Louis, MO, USA) and 10 µg/ml Blasticidine S hydrochloride (Sigma-Aldrich, St. Louis, MO, USA), while Free-Gfp mutants are treated with 20 µg/ml G 418.

Live cell experiment

Cells are concentrated to $c = 5x10^6$ cells/ml in shaking culture (150 rpm). 5h prior to the experiment, cells are washed with 17 µM K–Na phosphate buffered saline pH 6.0 (PBS, Sigma Aldrich, St. Louis, MO, USA). $c = 2.5x10^5$ cells/ml are introduced in the microfluidic chamber. cAMP at $c = 10^{-6}$ M is added as chemoattractant for measurements displayed in Fig. 6.2, and at $c = 2x10^{-4}$ M for measurements displayed in 8 and 9. PI3-Kinase was inhibited using 50 µM (0.17% DMSO) LY 294002 (L9908, Sigma-Aldrich, St. Louis, MO, USA). Measurements are performed with cells starved for $5 - 7$ h. Cell center of mass is extracted using the CellEvaluator algorithm [98]. Velocity and angle distributions in Fig. 6.2 are calculated over 10 frames, with a frame rate of $(2.5\,\mathrm{s})^{-1}$. A frame rate of $(2\,\mathrm{s})^{-1}$ is used for FDM and eccentricity analysis in 8 and 9. Cell eccentricity is obtained using the 'regionprops' function in Matlab 2010a (Mathworks, Ismaning, Germany).

Finite element computation (FEC)

For all numerical calculations, at least 70,000 gridpoints in 2d and 200,000 gridpoints in 3d are used; all calculations are performed with COMSOL Multiphysics 3.5 (Mathworks, Ismaning, Germany). The hydrodynamic velocity field is computed using the Stokes equation, the concentration field using the convection-diffusion equation. No-slip boundary conditions are used at the side walls. A constant inflow speed of 300 µm/s in the side flows and 250 µm/s in the central flow is assumed in the calculations. Vanishing viscous stress is assumed as boundary condition for the outflow. A diffusion coefficient of $5x10$ m²/s, no concentration flux boundary conditions at the walls, a relative chemoattractant concentration of 1 at the outer inlets and 0 at the inner inlet, are employed. The outflow of concentration is described

by a convective flux boundary condition, which allows for species transport by convection only.

Fluorescence dipolar moment (FDM) analysis

To extract the FDM (see sec. 7.2), the integrated product of the Gfp intensity FI of each pixel and its displacement from the cell center of mass d is plotted as a 2d vector. The home-made ImageJ plugin CellEvaluator [98] is used to find this center of mass. The FDM becomes positive if its vector points parallel to the direction of the gradient and negative if oriented in the opposite direction. Hence, the FDM (in analogy to an electric dipolar moment) yields the cell polarization, as identified by actin polymerization dynamics in Lim-Gfp cells. As the gradient direction in our setup switches in a defined axis, it is sufficient to use the amplitude of the resulting vector. The FDM is then normalized so that all cells exhibit comparable FDM values. High overall cell fluorescence intensity I will result in large FDM values and an increase in area R^2 ($R =$ cell radius) will add more pixels counting towards the FDM and an increase in the maximal pixel displacement R. We found the normalization with $I \cdot R^{3/2}$ to account best for cell individuality.

Bibliography

[1] L. Coultas, K. Chawengsaksophak, and J. Rossant. Endothelial cells and vegf in vascular development. *Nature*, 438(7070):937–945, 2005.

[2] J. Yu, J. Xiao, R. Xiaojia, K. Lao, and S. Xie. Probing gene expression in live cells, one protein molecule at a time. *Sciencel*, 311:1600–1603, 2006.

[3] J. P. Rieu, C. Barentin, Y. Maeda, and Y. Sawada. Direct mechanical force measurements during the migration of dictyostelium slugs using flexible substrata. *Biophysical Journal*, 89(5):3563–3576, 2005.

[4] R. G. Endres and N. S. Wingreen. Accuracy of direct gradient sensing by single cells. *Proc Natl Acad Sci U S A*, 105(41):15749–54, 2008.

[5] R. Insall and N. Andrew. Chemotaxis in dictyostefium: how to walk straight using parallel pathways. *Current Opinion in Microbiology*, 10(6):578–581, 2007.

[6] R. Y. Tsien. The green fluorescent protein. *Annu Rev Biochem*, 67:509–44, 1998.

[7] M. B. Elowitz, A. J. Levine, E. D. Siggia, and P. S. Swain. Stochastic gene expression in a single cell. *Science*, 297(5584):1183–6, 2002.

[8] A. Samadani, J. Mettetal, and A. van Oudenaarden. Cellular asymmetry and individuality in directional sensing. *Proc Natl Acad Sci U S A*, 103(31):11549–54, 2006.

[9] Ann M. Rajnicek, Louise E. Foubister, and Colin D. McCaig. Prioritising guidance cues: Directional migration induced by substratum

contours and electrical gradients is controlled by a rho/cdc42 switch. *Developmental Biology*, 312(1):448–460, 2007.

[10] M. J. Sato, H. Kuwayama, W. N. van Egmond, A. L. Takayama, H. Takagi, P. J. van Haastert, T. Yanagida, and M. Ueda. Switching direction in electric-signal-induced cell migration by cyclic guanosine monophosphate and phosphatidylinositol signaling. *Proc Natl Acad Sci U S A*, 106(16):6667–72, 2009.

[11] C. M. Lo, H. B. Wang, M. Dembo, and Y. L. Wang. Cell movement is guided by the rigidity of the substrate. *Biophysical Journal*, 79(1):144–152, 2000.

[12] S. Jungbauer, H. J. Gao, J. P. Spatz, and R. Kemkemer. Two characteristic regimes in frequency-dependent dynamic reorientation of fibroblasts on cyclically stretched substrates. *Biophysical Journal*, 95(7):3470–3478, 2008.

[13] R. P. Futrelle. Dictyostelium chemotactic response to spatial and temporal gradients - theories of the limits of chemotactic sensitivity and of pseudo-chemotaxis. *Journal of Cellular Biochemistry*, 18(2):197–212, 1982.

[14] D. Zicha, G. A. Dunn, and A. F. Brown. A new direct-viewing chemotaxis chamber. *J Cell Sci*, 99 (Pt 4):769–75, 1991.

[15] S. Boyden. The chemotactic effect of mixtures of antibody and antigen on polymorphonuclear leucocytes. *J Exp Med*, 115:453–66, 1962.

[16] S. K. W. Dertinger, D. T. Chiu, N. L. Jeon, and G. M. Whitesides. Generation of gradients having complex shapes using microfluidic networks. *Analytical Chemistry*, 73(6):1240–1246, 2001.

[17] D. Irimia, S. Y. Liu, W. G. Tharp, A. Samadani, M. Toner, and M. C. Poznansky. Microfluidic system for measuring neutrophil migratory responses to fast switches of chemical gradients. *Lab on a Chip*, 6(2):191–198, 2006.

[18] H. Kress, J. G. Park, C. O. Mejean, J. D. Forster, J. Park, S. S. Walse, Y. Zhang, D. Q. Wu, O. D. Weiner, T. M. Fahmy, and E. R.

Dufresne. Cell stimulation with optically manipulated microsources. *Nature Methods*, 6(12):905–909, 2009.

[19] B. Kuczenski, W. C. Ruder, W. C. Messner, and P. R. Leduc. Probing cellular dynamics with a chemical signal generator. *PLoS One*, 4(3):e4847, 2009.

[20] C. Beta, D. Wyatt, W. J. Rappel, and E. Bodenschatz. Flow photolysis for spatiotemporal stimulation of single cells. *Analytical Chemistry*, 79(10):3940–3944, 2007.

[21] S. Takayama, E. Ostuni, P. LeDuc, K. Naruse, D. E. Ingber, and G. M. Whitesides. Laminar flows - subcellular positioning of small molecules. *Nature*, 411(6841):1016–1016, 2001.

[22] D. B. Weibel and G. M. Whitesides. Applications of microfluidics in chemical biology. *Current Opinion in Chemical Biology*, 10(6):584–591, 2006.

[23] M. Baggiolini. Chemokines and leukocyte traffic. *Nature*, 392(6676):565–8, 1998.

[24] A. Bagorda, V. A. Mihaylov, and C. A. Parent. Chemotaxis: moving forward and holding on to the past. *Thrombosis and Haemostasis*, 95(1):12–21, 2006.

[25] C. Janetopoulos and R. A. Firtel. Directional sensing during chemotaxis. *Febs Letters*, 582(14):2075–2085, 2008.

[26] R. J. Petrie, A. D. Doyle, and K. M. Yamada. Random versus directionally persistent cell migration. *Nat Rev Mol Cell Biol*, 10(8):538–49, 2009.

[27] P. Pan, J. T. Bonner, and E. M. Hall. Folic-acid as second chemotactic substance in cellular slime molds. *Nature New Biology*, 237(75):181–182, 1972.

[28] P. Devreotes. Dictyostelium-discoideum - a model system for cell-cell interactions in development. *Science*, 245(4922):1054–1058, 1989.

[29] J. S. King and R. H. Insall. Chemotaxis: finding the way forward with dictyostelium. *Trends Cell Biol*, 19(10):523–30, 2009.

[30] L. Eichinger, J. A. Pachebat, G. Glockner, M. A. Rajandream, R. Sucgang, M. Berriman, J. Song, R. Olsen, K. Szafranski, Q. Xu, B. Tunggal, S. Kummerfeld, M. Madera, B. A. Konfortov, F. Rivero, A. T. Bankier, R. Lehmann, N. Hamlin, R. Davies, P. Gaudet, P. Fey, K. Pilcher, G. Chen, D. Saunders, E. Sodergren, P. Davis, A. Kerhornou, X. Nie, N. Hall, C. Anjard, L. Hemphill, N. Bason, P. Farbrother, B. Desany, E. Just, T. Morio, R. Rost, C. Churcher, J. Cooper, S. Haydock, N. van Driessche, A. Cronin, I. Goodhead, D. Muzny, T. Mourier, A. Pain, M. Lu, D. Harper, R. Lindsay, H. Hauser, K. James, M. Quiles, M. Madan Babu, T. Saito, C. Buchrieser, A. Wardroper, M. Felder, M. Thangavelu, D. Johnson, A. Knights, H. Loulseged, K. Mungall, K. Oliver, C. Price, M. A. Quail, H. Urushihara, J. Hernandez, E. Rabbinowitsch, D. Steffen, M. Sanders, J. Ma, Y. Kohara, S. Sharp, M. Simmonds, S. Spiegler, A. Tivey, S. Sugano, B. White, D. Walker, J. Woodward, T. Winckler, Y. Tanaka, G. Shaulsky, M. Schleicher, G. Weinstock, A. Rosenthal, E. C. Cox, R. L. Chisholm, R. Gibbs, W. F. Loomis, M. Platzer, R. R. Kay, J. Williams, P. H. Dear, A. A. Noegel, B. Barrell, and A. Kuspa. The genome of the social amoeba dictyostelium discoideum. *Nature*, 435(7038):43–57, 2005.

[31] L. Kreppel, P. Fey, P. Gaudet, E. Just, W. A. Kibbe, R. L. Chisholm, and A. R. Kimmel. dictybase: a new dictyostelium discoideum genome database. *Nucleic Acids Res*, 32(Database issue):D332–3, 2004.

[32] R. G. Endres and N. S. Wingreen. Accuracy of direct gradient sensing by cell-surface receptors. *Prog Biophys Mol Biol*, 100(1-3):33–9, 2009.

[33] P. R. Fisher, R. Merkl, and G. Gerisch. Quantitative-analysis of cell motility and chemotaxis in dictyostelium-discoideum by using an image-processing system and a novel chemotaxis chamber providing stationary chemical gradients. *Journal of Cell Biology*, 108(3):973–984, 1989.

[34] A. Bagorda and C. A. Parent. Eukaryotic chemotaxis at a glance. *Journal of Cell Science*, 121(16):2621–2624, 2008.

[35] P. A. Iglesias and P. N. Devreotes. Navigating through models of chemotaxis. *Current Opinion in Cell Biology*, 20(1):35–40, 2008.

[36] L. Ma, C. Janetopoulos, L. Yang, P. N. Devreotes, and P. A. Iglesias. Two complementary, local excitation, global inhibition mechanisms acting in parallel can explain the chemoattractant-induced regulation of pi(3,4,5)p-3 response in dictyostelium cells. *Biophysical Journal*, 87(6):3764–3774, 2004.

[37] C. Arrieumerlou and T. Meyer. A local coupling model and compass parameter for eukaryotic chemotaxis. *Developmental Cell*, 8(2):215–227, 2005.

[38] M. P. Neilson, D. M. Veltman, P. J. van Haastert, S. D. Webb, J. A. Mackenzie, and R. H. Insall. Chemotaxis: a feedback-based computational model robustly predicts multiple aspects of real cell behaviour. *PLoS Biol*, 9(5):e1000618.

[39] Y. Xiong, C. H. Huang, P. A. Iglesias, and P. N. Devreotes. Cells navigate with a local-excitation, global-inhibition-biased excitable network. *Proc Natl Acad Sci U S A*, 107(40):17079–86.

[40] L. Bosgraaf and P. J. Van Haastert. Navigation of chemotactic cells by parallel signaling to pseudopod persistence and orientation. *PLoS One*, 4(8):e6842, 2009.

[41] R. R. Kay, P. Langridge, D. Traynor, and O. Hoeller. Changing directions in the study of chemotaxis. *Nat Rev Mol Cell Biol*, 9(6):455–63, 2008.

[42] D. Botstein, S. A. Chervitz, and J. M. Cherry. Yeast as a model organism. *Science*, 277(5330):1259–60, 1997.

[43] J. G. Williams. Dictyostelium finds new roles to model. *Genetics*, 185(3):717–26.

[44] G. Gerisch, D. Hulser, D. Malchow, and U. Wick. Cell communication by periodic cyclic-amp pulses. *Philosophical Transactions of the Royal Society of London Series B-Biological Sciences*, 272(915):181, 1975.

[45] J. T. Bonner. A way of following individual cells in the migrating slugs of dictyostelium discoideum. *Proc Natl Acad Sci U S A*, 95(16):9355–9, 1998.

[46] K. F. Swaney, C.-H. Huang, and P. N. Devreotes. Eukaryotic chemotaxis: A network of signaling pathways controls motility, directional sensing, and polarity. *Annu. Rev. Biophys.*, 39:265–289, 2010.

[47] K. S. K. Uchida, T. Kitanishi-Yumura, and S. Yumura. Myosin ii contributes to the posterior contraction and the anterior extension during the retraction phase in migrating dictyostelium cells. *Journal of Cell Science*, 116(1):51–60, 2003.

[48] R. H. Insall and O. D. Weiner. Pip3, pip2, and cell movement–similar messages, different meanings? *Dev Cell*, 1(6):743–7, 2001.

[49] H. M. Loovers, M. Postma, I. Keizer-Gunnink, Y. E. Huang, P. N. Devreotes, and P. J. M. van Haastert. Distinct roles of pi(3,4,5)p-3 during chemoattractant signaling in dictyostelium: A quantitative in vivo analysis by inhibition of pi3-kinase. *Molecular Biology of the Cell*, 17(4):1503–1513, 2006.

[50] D. Wessels, D. F. Lusche, S. Kuhl, P. Heid, and D. R. Soll. Pten plays a role in the suppression of lateral pseudopod formation during dictyostelium motility and chemotaxis. *Journal of Cell Science*, 120(15):2517–2531, 2007.

[51] P. Devreotes and C. Janetopoulos. Eukaryotic chemotaxis: Distinctions between directional sensing and polarization. *Journal of Biological Chemistry*, 278(23):20445–20448, 2003.

[52] E. L. de Hostos. The coronin family of actin-associated proteins. *Trends Cell Biol*, 9(9):345–50, 1999.

[53] T. D. Pollard and G. G. Borisy. Cellular motility driven by assembly and disassembly of actin filaments. *Cell*, 112(4):453–65, 2003.

[54] L. F. Chen, C. Janetopoulos, Y. E. Huang, M. Iijima, J. Borleis, and P. N. Devreotes. Two phases of actin polymerization display different dependencies on pi(3,4,5)p-3 accumulation and have unique roles during chemotaxis. *Molecular Biology of the Cell*, 14(12):5028–5037, 2003.

[55] M. Etzrodt, H. C. F. Ishikawa, J. Dalous, A. Muller-Taubenberger, T. Bretschneider, and G. Gerisch. Time-resolved responses to chemoattractant, characteristic of the front and tall of dictyostelium cells. *Febs Letters*, 580(28-29):6707–6713, 2006.

[56] O. D. Weiner. Regulation of cell polarity during eukaryotic chemotaxis: the chemotactic compass. *Current Opinion in Cell Biology*, 14(2):196–202, 2002.

[57] M. Kollmann, L. Lovdok, K. Bartholome, J. Timmer, and V. Sourjik. Design principles of a bacterial signalling network. *Nature*, 438(7067):504–507, 2005.

[58] P. J. M. Van Haastert and P. N. Devreotes. Chemotaxis: Signalling the way forward. *Nature Reviews Molecular Cell Biology*, 5(8):626–634, 2004.

[59] F. Sanchez-Madrid and J. M. Serrador. Bringing up the rear: defining the roles of the uropod. *Nat Rev Mol Cell Biol*, 10(5):353–9, 2009.

[60] J. Franca-Koh, Y. Kamimura, and P. Devreotes. Navigating signaling networks: chemotaxis in dictyostelium discoideum. *Curr Opin Genet Dev*, 16(4):333–8, 2006.

[61] P. G. Charest and R. A. Firtel. Feedback signaling controls leading-edge formation during chemotaxis. *Current Opinion in Genetics and Development*, 16(4):339–347, 2006.

[62] N. Ibarra, A. Pollitt, and R. H. Insall. Regulation of actin assembly by scar/wave proteins. pages 1243–1246. Portland Press Ltd, 2005. ISI Document Delivery No.: 993CR Times Cited: 25 Cited Reference Count: 38.

[63] S. Funamoto, R. Meili, S. Lee, L. Parry, and R. A. Firtel. Spatial and temporal regulation of 3-phosphoinositides by pi 3-kinase and pten mediates chemotaxis. *Cell*, 109(5):611–23, 2002.

[64] S. Yumura and Y. Fukui. Reversible cyclic amp-dependent change in distribution of myosin thick filaments in dictyostelium. *Nature*, 314(6007):194–196, 1985.

[65] D. M. Veltman and P. J. Van Haastert. Guanylyl cyclase protein and cgmp product independently control front and back of chemotaxing dictyostelium cells. *Mol Biol Cell*, 17(9):3921–9, 2006.

[66] L. Bosgraaf and P. J. M. Van Haastert. A model for cgmp signal transduction in dictyostelium in perspective of 25 years of cgmp research. *Journal of Muscle Research and Cell Motility*, 23(7-8):781–791, 2002.

[67] P. G. Charest and R. A. Firtel. Big roles for small gtpases in the control of directed cell movement. *Biochem J*, 401(2):377–90, 2007.

[68] M. Postma, L. Bosgraaf, H. M. Loovers, and P. J. M. Van Haastert. Chemotaxis: signalling modules join hands at front and tail. *Embo Reports*, 5(1):35–40, 2004.

[69] M. J. Caterina and P. N. Devreotes. Molecular insights into eukaryotic chemotaxis. *Faseb Journal*, 5(15):3078–3085, 1991.

[70] R. A. Firtel and C. Y. Chung. The molecular genetics of chemotaxis: sensing and responding to chemoattractant gradients. *Bioessays*, 22(7):603–15, 2000.

[71] L. Bosgraaf, I. Keizer-Gunnink, and P. J. Van Haastert. Pi3-kinase signaling contributes to orientation in shallow gradients and enhances speed in steep chemoattractant gradients. *J Cell Sci*, 121(Pt 21):3589–97, 2008.

[72] O. Hoeller and R. R. Kay. Chemotaxis in the absence of pip3 gradients. *Current Biology*, 17(9):813–817, 2007.

[73] Y. Kamimura, Y. Xiong, P. A. Iglesias, O. Hoeller, P. Bolourani, and P. N. Devreotes. Pip3-independent activation of torc2 and pkb at the

cell's leading edge mediates chemotaxis. *Curr Biol*, 18(14):1034–43, 2008.

[74] D. M. Veltman, I. Keizer-Gunnik, and P. J. Van Haastert. Four key signaling pathways mediating chemotaxis in dictyostelium discoideum. *J Cell Biol*, 180(4):747–53, 2008.

[75] P. J. van Haastert, I. Keizer-Gunnink, and A. Kortholt. Essential role of pi3-kinase and phospholipase a2 in dictyostelium discoideum chemotaxis. *J Cell Biol*, 177(5):809–16, 2007.

[76] R. H. Insall. Understanding eukaryotic chemotaxis: a pseudopod-centred view. *Nat Rev Mol Cell Biol*, 11(6):453–8.

[77] P. J. M. van Haastert. A stochastic model for chemotaxis based on the ordered extension of pseudopods. *Biophysical Journal*, 99:3345–3354, 2010.

[78] L. Bosgraaf and P. J. Van Haastert. The ordered extension of pseudopodia by amoeboid cells in the absence of external cues. *PLoS One*, 4(4):e5253, 2009.

[79] A. J. Bae, C. Beta, and E. Bodenschatz. Rapid switching of chemical signals in microfluidic devices. *Lab Chip*, 9(21):3059–65, 2009.

[80] D. Muzzey and A. van Oudenaarden. Quantitative time-lapse fluorescence microscopy in single cells. *Annu Rev Cell Dev Biol*, 252(3):864–865, 1977.

[81] O. Brandman and T. Meyer. Feedback loops shape cellular signals in space and time. *Science*, 322(5900):390–395, 2008.

[82] Takanari Inoue and Tobias Meyer. Synthetic activation of endogenous pi3k and rac identifies an and-gate switch for cell polarization and migration. *PLoS One*, 3(8):Article No.: e3068, 2008.

[83] O. D. Weiner, W. A. Marganski, L. F. Wu, S. J. Altschuler, and M. W. Kirschner. An actin-based wave generator organizes cell motility. *Plos Biology*, 5(9):2053–2063, 2007.

[84] G. Schwake, S. Youssef, J. T. Kuhr, S. Gude, M. P. David, E. Mendoza, E. Frey, and J. O. Radler. Predictive modeling of non-viral gene transfer. *Biotechnol Bioeng*, 105(4):805–13.

[85] Madeleine Leisner, Kerstin Sting, Erwin Frey, and Berenike Maier. Stochastic switching to competence. *Current Opinion in Microbiology*, 11(6):553–559, 2008.

[86] B. Meier, A. Zielinski, C. Weber, D. Arcizet, S. Youssef, T. Franosch, J. O. Radler, and D. Heinrich. Chemotactic cell trapping in controlled alternating gradient fields. *Proc Natl Acad Sci U S A*.

[87] A. E. Kamholz, E. A. Schilling, and P. Yager. Optical measurement of transverse molecular diffusion in a microchannel. *Biophysical Journal*, 80(4):1967–1972, 2001.

[88] A. E. Kamholz, B. H. Weigl, B. A. Finlayson, and P. Yager. Quantitative analysis of molecular interaction in a microfluidic channel: The t-sensor. *Analytical Chemistry*, 71(23):5340–5347, 1999.

[89] A. E. Kamholz and P. Yager. Molecular diffusive scaling laws in pressure-driven microfluidic channels: deviation from one-dimensional einstein approximations. *Sensors and Actuators B-Chemical*, 82(1):117–121, 2002.

[90] M. Dworkin and K. H. Keller. Solubility and diffusion coefficient of adenosine 3,5-monophosphate. *J. Biol. Chem.*, 252:301–27, 2009.

[91] C. C. Chang, Z. X. Huang, and R. J. Yang. Three-dimensional hydrodynamic focusing in two-layer polydimethylsiloxane (pdms) microchannels. *Journal of Micromechanics and Microengineering*, 17(8):1479–1486, 2007.

[92] S. Fache, J. Dalous, M. Engelund, C. Hansen, F. Chamaraux, B. Fourcade, M. Satre, P. Devreotes, and F. Bruckert. Calcium mobilization stimulates dictyostelium discoideum shear-flow-induced cell motility. *Journal of Cell Science*, 118(15):3445–3457, 2005.

[93] J. Dalous, E. Burghardt, A. Muller-Taubenberger, F. Bruckert, G. Gerisch, and T. Bretschneider. Reversal of cell polarity and actin-myosin cytoskeleton reorganization under mechanical and chemical stimulation. *Biophysical Journal*, 94(3):1063–1074, 2008.

[94] C. Beta, T. Frohlich, H. U. Bodeker, and E. Bodenschatz. Chemotaxis in microfluidic devices - a study of flow effects. *Lab on a Chip*, 8(7):1087–1096, 2008.

[95] C. G. Galbraith, R. Skalak, and S. Chien. Shear stress induces spatial reorganization of the endothelial cell cytoskeleton. *Cell Motil. Cytoskeleton*, 40:317–330, 1998.

[96] R. Zaidel-Bar, Z. Kam, and B. Geiger. Polarized down regulation of the paxillin-p130-rac1 pathway induced by shear flow. *J. Cell Sci.*, 109:3997–4007, 2005.

[97] E. Decave, D. Rieu, J. Dalous, S. Fache, Y. Brechet, B. Fourcade, M. Satre, and F. Bruckert. Shear flow-induced motility of dictyostelium discoideum cells on solid substrate. *Journal of Cell Science*, 116(21):4331–4343, 2003.

[98] S. Youssef, S. Gude, and J. O. Radler. Automated tracking in live-cell time-lapse movies. *Integr Biol (Camb)*, 2011.

[99] S. Zhang, P. G. Charest, and R. A. Firtel. Spatiotemporal regulation of ras activity provides directional sensing. *Curr Biol*, 18(20):1587–93, 2008.

[100] L. Li, S. F. Norrelykke, and E. C. Cox. Persistent cell motion in the absence of external signals: a search strategy for eukaryotic cells. *PLoS One*, 3(5):e2093, 2008.

[101] P. J. Van Haastert. Chemotaxis: insights from the extending pseudopod. *J Cell Sci*, 123(Pt 18):3031–7, 2010.

[102] L. Bosgraaf and P. J. Van Haastert. Navigation of chemotactic cells by parallel signaling to pseudopod persistence and orientation. *PLoS One*, 4(8):e6842, 2009.

[103] E. C. Rericha and C. A. Parent. Steering in quadruplet: the complex signaling pathways directing chemotaxis. *Sci Signal*, 1(22):pe26, 2008.

[104] M. Westphal, A. Jungbluth, M. Heidecker, B. Muhlbauer, C. Heizer, J. M. Schwartz, G. Marriott, and G. Gerisch. Microfilament dynamics during cell movement and chemotaxis monitored using a gfp-actin fusion protein. *Curr Biol*, 7(3):176–83, 1997.

[105] J. Prassler, A. Murr, and G. Marriott. Ddlim is a cytoskeleton associated protein involved in the protrusion of lamellipodia. *Molecular Biology of the Cell*, 8(SUPPL.):61A, 1997.

[106] N. Andrew and R. H. Insall. Chemotaxis in shallow gradients is mediated independently of ptdins 3-kinase by biased choices between random protrusions. *Nat Cell Biol*, 9(2):193–200, 2007.

[107] L. F. Chen, M. Iijima, M. Tang, M. A. Landree, Y. E. Huang, Y. Xiong, P. A. Iglesias, and P. N. Devreotes. Pla(2) and pi3k/pten pathways act in parallel to mediate chemotaxis. *Developmental Cell*, 12(4):603–614, 2007.

[108] M. A. Unger, H.-P. Chou, T. Thorsen, A. Scherer, and S. R. Quake. Monolithic microfabricated valves and pumps by multilayer soft lithography. *Science*, 288:113–116, 2000.

[109] G. Charras and E. Paluch. Blebs lead the way: how to migrate without lamellipodia. *Nature*, 9:730–736, 2008.

[110] P. D. Langridge and R. R. Kay. Blebbing of dictyostelium cells in response to chemoattractant. *Exp. Cell Res.*, 312:2009–2017, 2006.

[111] D. Gabriel, U. Hacker, J. Koehler, A. Mueller-Taubenberger, J.M Schwartz, M. Westphal, and G. Gerisch. The contractile vacuole network of dictyostelium as a distinct organelle: its dynamics visualized by a gfp marker protein. *J. Cell Sci.*, 112:3995–4005, 1999.

[112] T. Bretschneider, S. Diez, K. Anderson, J. Heuser, M. Clarke, A. Mueller-Taubenberger, J. Koehler, and G. Gerisch. Dynamic actin patterns and arp2/3 assembly at the substrate-attached surface of motile cells. *Curr. Biol.*, 14:1–10, 2004.

List of Figures

Abbreviations

CGG	Chemotactic Gradient Generator
FDM	Fluorescence Distribution Moment
PI3-Kinase	Phosphoinositide 3-kinases
PlA2	Phospholipase A2
PTEN	Phosphatase and Tensin homolog
cGMP	Cyclic guanosine monophosphate
cAMP	cyclic Adenosin-3´,5´-monophosphat
PIP2	Phosphatidylinositol (4,5)-bisphosphate
PIP3	Phosphatidylinositol (3,4,5)-trisphosphate
F-actin	filamentous actin
cAR	cAMP receptor
FEC	Finite Element Calculation
LY	LY 294002

Associated Publications

D. Arcizet, B. Meier, E. Sackmann, J. O. Rädler and D. Heinrich
Temporal Analysis of Active and Passive Transport in Living Cells
Phys. Rev. Lett. 101, 248103 (2008)
Virtual Journal of Biological Physics Research, published on December 15 (2008)

B. Meier, A. Zielinski, C. Weber, D. Arcizet, S. Youssef, T. Franosch, J. O. Rädler and D. Heinrich
Chemotactic Cell Trapping in Alternating Gradient Fields
Proc. Natl. Acad. Sci. 108(28):11417-11422 (2011)
Faculty of 1000 , evaluated by Prof. R. Firtel (UCSD)

L. Tweedy, B. Meier, J. Stephan, D. Heinrich and R. Endres
Cell shape and behaviour for accurate chemotaxis
in preparation

Danke an ...

Joachim Rädler, für die Möglichkeit meine Doktorarbeit an deinem Lehrstuhl durch zu führen, mein tolles Thema, die Winterschule und die tolle Atmosphäre am Lehrstuhl.

Doris Heinrich, für die Betreuung meiner Doktorarbeit, für die lehrreichen Jahre und viele tolle Konferenzen.

Thomas Franosch, **Christoph Weber** und **Alejandro Zielinski**, für die gute Zusammenarbeit.

Volker, **Dave** und **Verena**, dafür dass niemals raus kommen wird wie konfus meine Gedanken sind und dass ich keine Ahnung von Grammatik haben tu.

Gerlinde, **Susi** und **Susi**, man mag sich gar nicht vorstellen wie die Experimente ohne Euch funktionieren sollten.

Margarete, dafür dass auch außerhalb des Labors alles funktioniert.

die **Rädlers**, für eine kurzweilige Zeit, viele interessante Diskussionen und Gespräche und viele gemeinsame Stunden am Kicker, Grill und im Labor natürlich. Oder wie man bei mir zu Hause sagt, dass alles gepasst hat.

meine **Eltern** und meine **Großmutter**, dafür dass ihr mich bis heute unterstützt und an mich glaubt.

Maria dass du es mit mir aushältst, und immer zur richtigen Zeit da bist.